

Volume 4 • Number 4 • October 2010
ISSN: 1557-7244

Journal of

**APPLIED
PACKAGING
RESEARCH**



Aim and Scope

The *Journal of Applied Packaging Research* is an international forum for the dissemination of research papers, review articles, tutorials and news about innovative or emerging technologies for the packaging industry. The journal is targeted towards the broad packaging community including packaging scientists and engineers in industry or academic research and development, food scientists and technologists, materials scientists, mechanical engineers, industrial and systems engineers, toxicologists, analytical chemists, environmental scientists, regulatory officers, and other professionals who are concerned with advances in the development and applications of packaging.

Co-Editors-in-Chief

Changfeng Ge

Packaging Science
Rochester Institute of Technology
One Memorial Drive
Rochester, NY 14623-5603
Phone: 585-475-5391
Email: cfgmet@rit.edu

Bruce Welt

Packaging Science
University of Florida, Box 110570
Gainesville, FL 32611-0570
Phone: 352-392-1864, X-111
Email: bwelt@ufl.edu

Editorial Advisory Board

Rafael Auras

Michigan State University

Larry Baner

Nestle Purina Pet Care

Heather P. Batt

Clemson University

Vanee Chonhenchob

Kasetart University, Thailand

Robert Clarke

Michigan State University

Lixin Lu

Jiangnan University, PR China

Gunilla Jönson

Lund University, Sweden

Lisa J. Mauer

Purdue University

Katsuhiko Saito

Kobe University, Japan

Jay Singh

Cal Poly State University

Fritz Yambrach

San Jose State University

JOURNAL OF APPLIED PACKAGING RESEARCH—Published quarterly—
January, April, July and October by DEStech Publications, Inc., 439 North Duke Street,
Lancaster, PA 17602-4967.

This journal is recommended by The National Institute of Packaging Handling and
Logistics Engineers (www.niphle.org).

Indexed by Chemical Abstracts Service.

Indexed and abstracted by Pira International.

Subscriptions: Annual \$319 (Print), \$319 (Electronic) and \$344 (Print and Electronic).
Single copy price \$95.00. Foreign subscriptions add \$45 per year for postage.

(ISSN 1557-7244)



DEStech Publications, Inc.

439 North Duke Street, Lancaster, PA 17602-4967, U.S.A.

©Copyright by DEStech Publications, Inc. 2010—All Rights Reserved

C O N T E N T S

Research

- Modified Simulated Drop Test for Transmitted Shock Characteristics of Structural Corrugated Fiber Board** 189
CHEN ZHONG and KATSUHIKO SAITO
- Life Cycle Inventory Comparison of Paper and Plastic Based Packaging Systems for Strawberry Distribution** 203
JAY SINGH and ARIC KRASOWSKI
- The Effect of Moisture Content on Compression Strength of Boxes Made of Solid Fiberboard with Polyethylene Coating—An Experimental Study** 223
SARA PAUNONEN and ØYVIND GREGERSEN
- Dynamics of Product-Transport-System by Improved Inverse Sub-structuring Method** 243
WANG JUN, LU LI-XIN and WANG ZHI-WEI
- Effect of Freeze-Thaw Cycling on the Compression Strength of Folding Cartons made from Different Materials** 257
KOUSHIK SAHA, BRUCE HARTE, GARY BURGESS and SUJEET ADUDODLA

Modified Simulated Drop Test for Transmitted Shock Characteristics of Structural Corrugated Fiber Board

CHEN ZHONG^{1,*} and KATSUHIKO SAITO²

¹*Graduate Student, Kobe University, Fukaeminami, Higashinada, Kobe, Japan*

²*Transport Packaging Laboratory, Kobe University, Fukaeminami, Higashinada, Kobe, Japan*

ABSTRACT: For structural cushioning materials, the drop test based on the traditional equivalent drop theory is usually performed. However, no researcher has dealt up the study that whether the modified equivalent drop theory is suitable for the structural cushioning materials. Thus, our study has focused on modifying the simulated drop test for transmitted shock characteristics of the structural cushioning materials. A sleeve cushion being made of a corrugated fiber board was used as a structural cushioning material, and the shock test and the dynamic compress test were performed in this study. Proof test showed that the modified equivalent drop theory can also be applied for structural corrugated fiber board.

INTRODUCTION

WITH the development of society, new cushioning materials have appeared constantly and been applied to the packaging field. Nevertheless, the corrugated fiber board is still widely used in transport packaging (such as corrugated carton) by far for its low cost, cushioning and environmental-friendly performances. Therefore, the test for the transmitted shock characteristics of the corrugated fiber board is an important issue.

According to JIS-Z-0240-2002 [1] [Structural Cushioning Materials for Packaging—Determination of Cushioning Performance] (this standard corresponds with ASTM-D4168-95 [2] [Standard Test Methods for Transmitted Shock Characteristics of Foam-in-Place Cushioning Materials]), the corrugated carton belongs to the structural cushioning

*Author to whom correspondence should be addressed. E-mail: 095w403w@stu.kobe-u.ac.jp

material, and the shock test based on the traditional equivalent drop theory (traditional theory) should be performed to test whose transmitted shock characteristics.

There were two correcting methods that are based on the new equivalent drop theory (modified theory) [3]: the correcting method-1—the method in which the input velocity change of the shock test is determined after solving the model's the natural frequency with no attenuation f_n and the damping ratio ξ according to the dynamic compression test; and the correcting method-2—the method in which the drop height of the dynamic compression test is determined after solving the model's f_n and ξ according to the shock test. It has been confirmed that the traditional theory had limits, and the modified theory was recommended for its well precision. Thus, it is the key step to calculate the correcting coefficient that relates to ξ when we apply the modified theory.

MATERIALS AND METHODS

1. Equivalent Drop Theory

1.1 Traditional Equivalent Drop Theory [4]

The structural cushioning materials are assumed to follow a linear spring-mass model (Figure 1), and the peak acceleration occurring on a weight dummy $A_{ff \max}$ of the dynamic compression test is shown as follows:

$$A_{ff \max} = \omega_n \cdot V \quad (1)$$

where ω_n is the natural angular frequency with no attenuation, and V is the velocity of the weight dummy.

For the shock test, when an extremely short half-sine shock pulse is

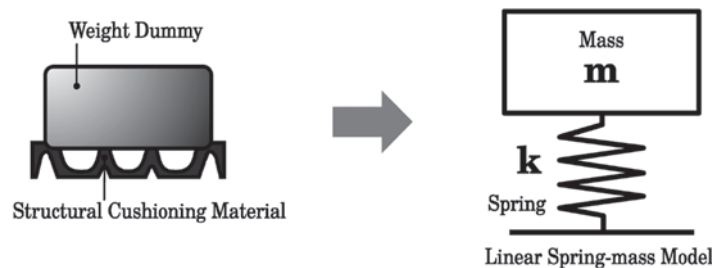


Figure 1. Traditional model.

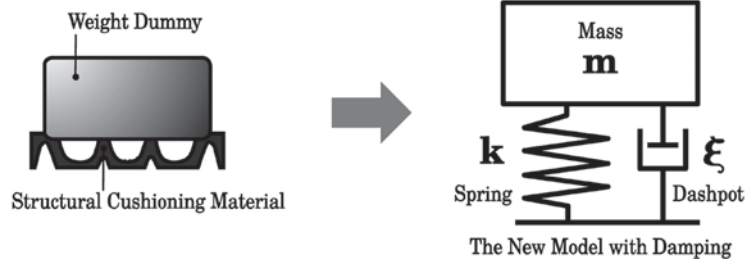


Figure 2. Attenuation model.

applied to the system, the peak acceleration of weight dummy $A_{cs \max}$ can be expressed as

$$A_{cs \max} = \omega_n \cdot V_c \quad (2)$$

where V_c is the velocity change on the shock table.

Comparing Equations (1) and (2), let $V = V_c$ when the dynamic compression test and the shock test are performed, then we know $A_{ff \max}$ equals $A_{cs \max}$.

1.2 Modified Equivalent Drop Theory [5]

Under the modified theory, a concept of the damping ratio ξ is introduced, and the structural cushioning material is assumed to obey a single degree of freedom attenuation model (Figure 2).

For the dynamic compression test, the peak acceleration occurring on the weight dummy $A_{ff \max}$ is

$$A_{ff \max} = n_{ff} \cdot \omega_n \cdot V \quad (3)$$

$$\therefore n_{ff} = \left| \frac{2\xi^2 - 1}{\sqrt{1 - \xi^2}} \right| \cdot \exp\left(\frac{-\pi\xi}{2\sqrt{1 - \xi^2}} \right) \quad (4)$$

where n_{ff} is the correction coefficient of the dynamic compression test [5].

Similarly, for the shock test, the peak acceleration of the weight dummy $A_{cs \max}$ is as follows:

$$A_{cs \max} = n_{cs} \cdot \omega_n \cdot V_c \quad (5)$$

$$\therefore n_{cs} = \frac{T_r}{2\pi \cdot f_n \cdot D_e} \quad (6)$$

where n_{cs} is the correction coefficient of the shock test, T_r is the shock transmissibility, and D_e is the effective impact duration.

According to Equations (3) and (5), we can see that a condition— n_{ff}/n_{cs} or n_{cs}/n_{ff} —must be considered if we want the dynamic compression test and the shock test to be equivalent under the new attenuation model. Here n_{ff}/n_{cs} and n_{cs}/n_{ff} are called the *correction coefficient*.

2. Test Equipment and Materials

The dynamic compression tester, the shock machine, the “shock manager” instrument were used in this study, and the connection between them is shown in Figure 3.

The corrugated fiber board (A flute) whose size is $110 \times 110 \times 50$ mm was used as the test material after being folded into a shape of a sleeve (Figure 4). An iron panel whose size is $150 \times 150 \times 22$ mm and weight is 4 kgf was used as the weight dummy (Figure 5).

3. Test Condition and Test Setup

- Equivalent free-fall height:

According to JIS-Z-0240-2002, an equivalent free-fall height h was set at 60 cm.

- Low-pass filtering:

According to JIS-Z-0240-2002, 300 Hz low-pass filtering is recommended for the test of the structural cushioning materials, thus 300 Hz low-pass filtering was applied.

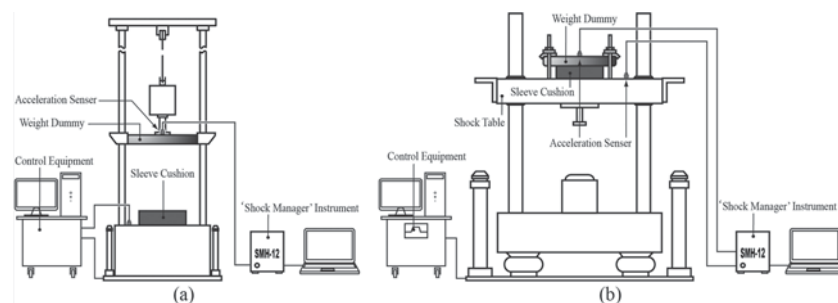


Figure 3. Illustration of connection between the test equipment. (a) The dynamic compression test, (b) the shock test.

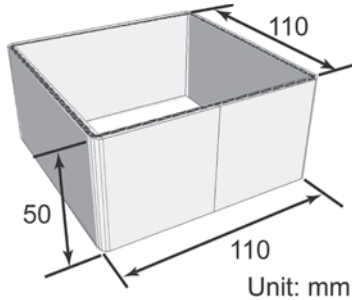


Figure 4. Sleeve cushion.

- Pretreatment of the test materials:

The test materials were placed in a controlled atmospheric condition where the temperature was 23°C and the relative humidity was 50% for 24 hours.

- Acceleration sensor and weight dummy:

The weight dummy used in both tests was the same weight (4 kgf), and the acceleration sensor used for measuring the peak acceleration was fixed in the center above the weight dummy in both tests (Figure 5).

- Data collection:

When $h = 60$ cm, we can calculate that the theoretical velocity is 3.43 m/s using the formula $V = \sqrt{2gh}$.

For the dynamic compression test, the setup drop height was adjusted repeatedly until the velocity of the weight dummy become 3.43 m/s; For the shock test, an adjusting function in the controlling

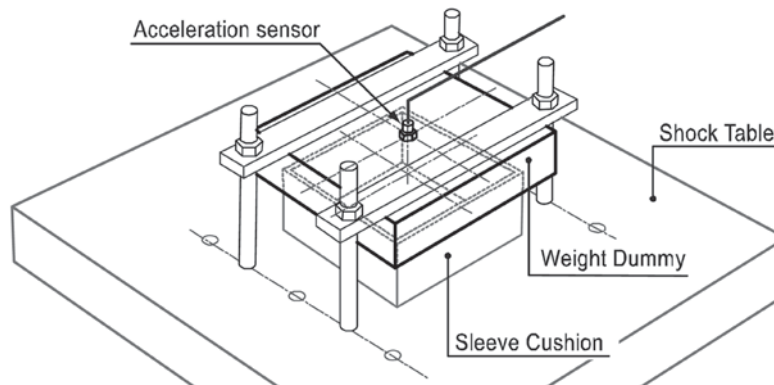


Figure 5. Acceleration sensor and weight dummy (shock test).

software was used by repetition until the velocity change occurring on the shock table changed to 3.43 m/s. For both tests, the data were effective only when $V = 3.43$ m/s or $V_c = 3.43$ m/s, and 10 times data were collected for each test.

4. Correcting Method-1

In order to calculate the velocity change V_c , n_{ff} and n_{cs} should be calculated respectively.

4.1 Calculation of n_{ff}

After the dynamic compression test was performed using the corrugated fiber board as the test material, the response acceleration-time curve was obtained as shown in Figure 6. We can see that the waveform of the result was not a smooth line with one maximum value, but was a zigzag shape.

For the dynamic compression test, we know

$$D = \frac{T_d}{2} = \frac{\pi}{\omega_n \sqrt{1 - \xi^2}} \quad (7)$$

where D is the impact duration, and T_d is the period of a shock.

Combining Equation (7) with Equations (3) and (4), we obtain

$$\frac{A_{ff \max} \cdot D}{\pi V_c} = \pm \frac{2\xi^2 - 1}{1 - \xi^2} \cdot \exp\left(\frac{-\pi\xi}{2\sqrt{1 - \xi^2}}\right) \quad (8)$$

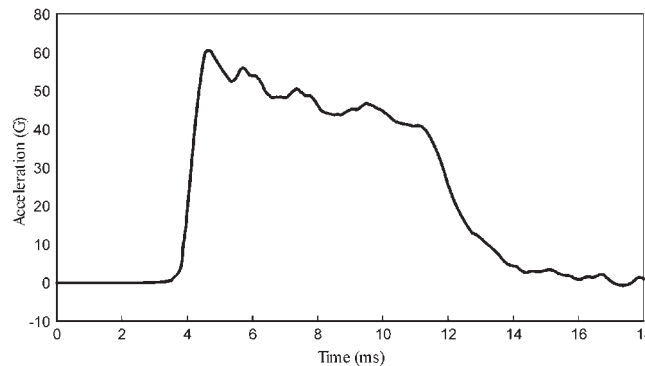


Figure 6. Response acceleration-time curve (Corrugated board sleeve).

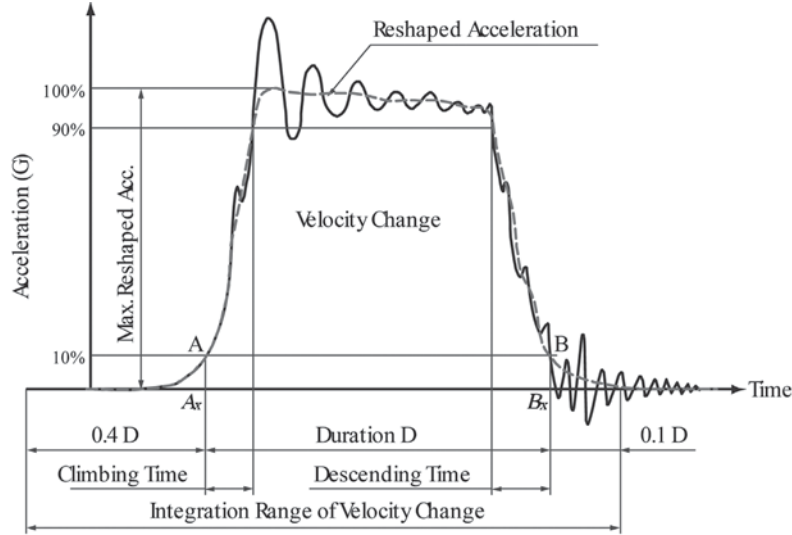


Figure 7. Illustration of impact duration D [6].

where “-” is valid for $\xi < 0.707$, and “+” for $\xi > 0.707$. For the convenience of the next statement, Equation (8) is split into two functions:

$$F_1 = \frac{A_{ff \max} \cdot D}{\pi V_c}$$

and

$$F_2 = \pm \frac{2\xi^2 - 1}{1 - \xi^2} \cdot \exp\left(\frac{-\pi\xi}{2\sqrt{1 - \xi^2}}\right)$$

For the shock test, there is a recommendation in JIS-Z-0119-2002 [6] [Mechanical-shock fragility testing methods for packaging and products design] (this standard corresponds with ISO-8568-1989 [7] [Mechanical shock—Testing machines—Characteristics and performance]): For the impact acceleration, because of the effect of the high frequency wave, the target wave which is measured by the acceleration sensor becomes unsmooth. Therefore, the equalization process to the amplitude of high frequency wave has to perform to draw a reference line that has an equal distance to both sides of wave ridges. This approach is called reshape acceleration process, and the maximum acceleration after being reshaped is called max. reshaped acceleration (Figure 7).

According to Figure 7, D can be obtained using the method as follows: First, for the metadata of tests, the reshaped acceleration curve

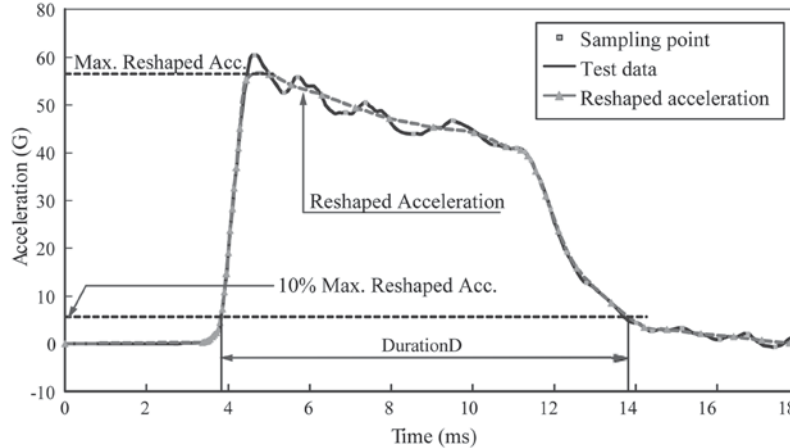


Figure 8. Reshaped acceleration.

can be plotted and the max. reshaped acceleration be obtained after the reshape acceleration process is run. Subsequently, a horizontal line is drawn from the position whose ordinate equals 10% max. reshaped acceleration, and it intersects the reshaped acceleration curve at two points A and B. D can be obtained after the x coordinate of B subtracts that of A. Hence, the reshape acceleration process is the key to the problem, and it is solvable with the method of a moving average.

The collected data were analyzed using data analysis software OriginPro 7.5 (OriginLab Inc., USA) to calculate the values of the moving

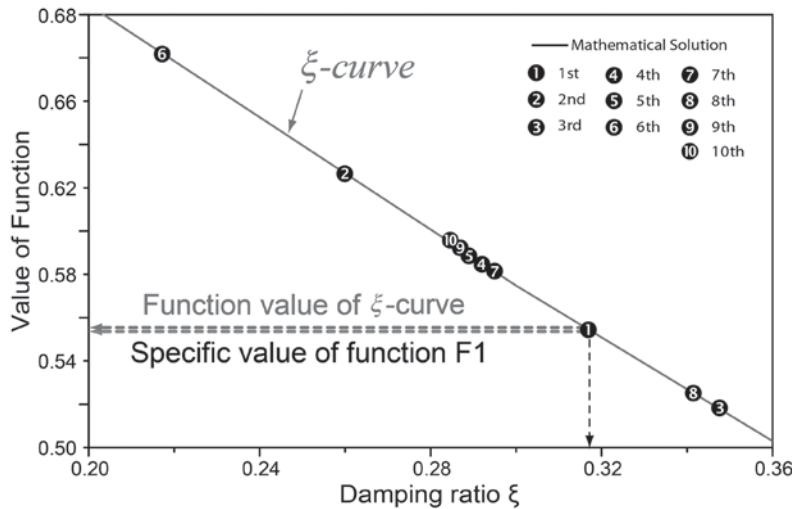


Figure 9. Calculation of the damping ratio ξ .

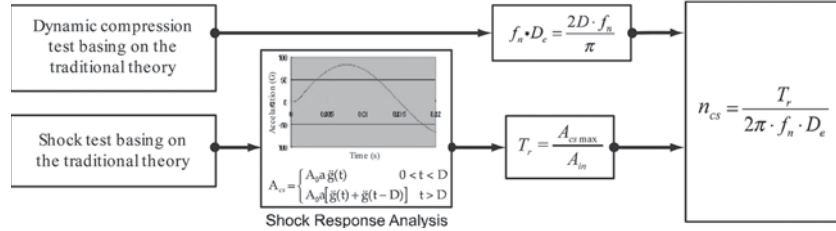


Figure 10. Calculation of n_{cs} .

average. Then, we plotted the figure of the reshaped acceleration curve and computed the value of the max. reshaped acceleration (Figure 8). Finally, D was calculated.

Using the function F_2 , a ξ -curve that relates to ξ can be plotted in the mathematics software such as Maple (Maplesoft Inc., Canada) (Figure 9). Furthermore, the metadata of $A_{ff\max}$, V_c , and D were imported into the function F_1 and the value of F_1 was calculated. The corresponding damping ratio ξ was available when these specific values of the function F_1 matched the function values of the ξ -curve (the error is smaller than 0.001). At last, n_{ff} can be calculated after ξ was imported into Equation (4). The result of ξ is shown in Figure 9.

4.2 Calculation of n_{cs}

n_{cs} can be computed using the shock response analysis [5] and Equation (6). The flowchart is shown in Figure 10.

Finally, the corrected velocity change V_c was calculated according to the formula $V_c = (n_{ff}/n_{cs})V$. After the velocity change V_c was corrected, the shock test was re-performed, and the new data of the peak accelerations were recorded.

5. Correcting Method-2 [3]

Using the data of the shock test that based on the traditional theory, the model's natural frequency f_n can be calculated, then n_{cs} was calculated. In addition, the shock response analysis was performed and n_{ff} was obtained. Subsequently, the equivalent drop height was derived. Finally, the corrected velocity V was calculated according to the formula $V = (n_{cs}/n_{ff})V_c$ (Figure 11).

Using the corrected velocity V , the dynamic compression test was re-performed, and the new data of the peak accelerations were obtained.

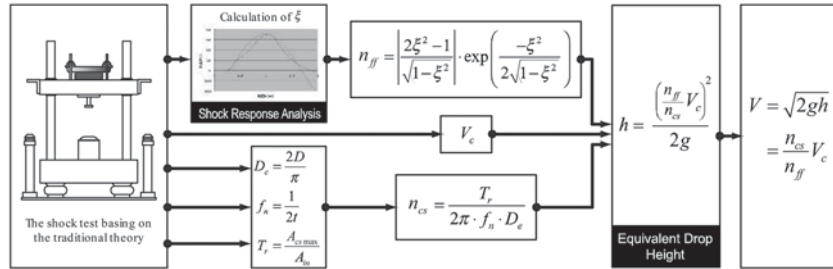


Figure 11. Flowchart of the correcting method-2.

6. Flow of the Tests

First, the dynamic compression test and the shock test were performed using the traditional method. Subsequently, on the basis of metadata of these two tests, n_{ff} and n_{cs} were calculated after computing ξ . Third, the corrected two tests were performed using the correction coefficient n_{ff}/n_{cs} or n_{cs}/n_{ff} respectively. Finally, the results of the two tests were compared to evaluate the feasibility of the modified theory for structural corrugated fiber board (Figure 12). According to the Section 4 and 5, it is known that n_{ff}/n_{cs} and n_{cs}/n_{ff} are not the simple reciprocal relations, but are completely different coefficients.

Here, the correcting method-1 is used as an example to explain the test flow concretely: First of all, the dynamic compression test and the shock test were carried out respectively under the traditional method. For the dynamic compression test, we measured the acceleration-time curve, the peak acceleration $A_{ff\max} = 61.80$ G (Table 1) and the velocity $V = 3.43$ m/s. Using the method of the moving average and Origin we calculated the duration $D = 9.92$ ms. Importing those data into the func-

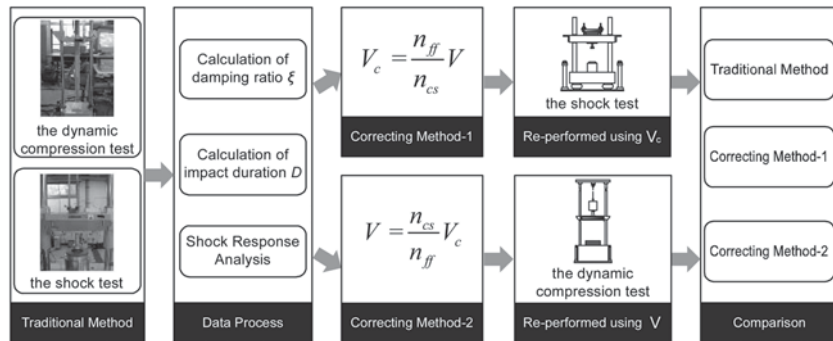


Figure 12. Flowchart of the tests.

Table 1. Comparison of the Peak Accelerations of the Two Tests (G-factor).

Order	Traditional Theory		Modified Theory	
	DC Test (G) ^a	Shock Test (G) ^b	Shock Test (G) ^c	DC Test (G) ^d
1	61.80	59.90	62.80	60.80
2	62.40	60.30	61.70	62.70
3	59.70	63.90	63.30	58.60
4	57.50	61.70	62.40	62.40
5	59.80	61.50	63.30	60.70
6	62.00	62.90	60.50	63.20
7	60.30	64.00	62.40	62.90
8	60.00	64.20	63.70	59.90
9	62.50	60.50	62.70	61.80
10	60.10	61.30	62.00	62.50
Average Value	60.61	62.02	61.55	62.48
Difference of Average Value		1.41	0.94	0.46

^aThe traditional method (DC test is the dynamic compression test).
^bThe traditional method.
^cThe correcting method-1.
^dThe correcting method-2.

tion F_1 , the value of F_1 was known as 0.5573, then we sought the point whose function value equals 0.5573 on the ξ -curve, and $\xi = 0.315$ was obtained. Using Equation (4) we knew $n_{ff} = 0.5014$ and $f_n = 53.13$. On the other hand, for the shock test, we measured the acceleration-time curve, the peak acceleration $A_{cs\ max} = 59.90$ G (Table 1), the maximum input acceleration $A_{in\ max} = 254$ G and the shock duration $D = 2.44$ ms. Using those data and f_n and ξ , the shock response analysis was carried out to calculate the response acceleration of the shock test $A_{cs\ max}$ and we got $A_{cs\ max} = 105.92$ G. We calculated $T_r = 0.4167$ by using $T_r = A_{cs\ max}/A_{in\ max}$. Finally, $n_{cs} = 0.8041$ was obtained after T_r was imported into Equation (6). At last, we calculated that the corrected velocity change of the shock test V_c should be 2.14 m/s according to the formula $V_c = (n_{ff}/n_{cs})V$. The shock test was re-performed by using the corrected V_c , and the revised peak acceleration of the shock test was measured as 62.80 G (Table 1).

Among the above parameters, n_{cs} , n_{ff} , ξ were calculated by equipment, and $A_{ff\ max}$, $A_{cs\ max}$, V , V_c , f_n , D were not associated with equipments.

RESULTS AND DISCUSSION

The values in Table 1 are the peak accelerations (G-factor) of the

weight dummy. The values from the left to the right are: the result of the dynamic compression test based on the traditional theory, the result of the shock test based on the traditional theory, the result of the shock test after being corrected by the correcting method-1, and the result of the dynamic compression test after being corrected by the correcting method-2. The average values of the data of the four experiments were calculated. Then, the difference of the average values were compared and the result is shown in the bottom of Table 1.

- The average values between the two tests based on the traditional theory were different, and this proved the limitations of the traditional theory.
- Comparing to column c and a, column d and b of Table 1, the peak accelerations were larger after V or V_c was corrected.
- The difference of the average value became gradually smaller from the traditional method to the correcting method-1 to the correcting method-2. Considering the effect of uniqueness of the sleeve cushion, although the results between the dynamic compress test and the shock test were different yet after modified by using the correction coefficient, both the correcting method-1 and the correcting method-2 have raised the equivalent precision of the two tests comparing the traditional method. In other words, the modified simulated drop test of the structural corrugated fiber board was improved after using the modified equivalent drop theory.
- The modifying effects of the two correcting methods were not the same, and the correcting method-2 was superior to the correcting method-1.

CONCLUSION

Excluding the effect of uniqueness of the sleeve cushion, the results of the dynamic compress test and the shock test were not the same due to the limitations of the traditional theory. Therefore, the effect of attenuation must be considered. For the structural corrugated fiber board, the equivalent precision of the simulated drop test can be improved after modified by the correcting methods based on the modified theory. According to the data of proof experiments, it can be said that the modified equivalent drop theory is also suitable for the structural corrugated fiber board.

REFERENCES

1. JIS-Z-0240-2002, *Structural Cushioning Materials for Packaging—Determination of Cushioning Performance*.
2. ASTM-D4168-95, *Standard Test Methods for Transmitted Shock Characteristics of Foam-in-Place Cushioning Materials*.
3. Chen ZHONG and Katsuhiko SAITO, Equivalent Drop Test Modification for Determination of Cushioning Performance, *Journal of Packaging Science & Technology, Japan*. Vol. 19, No. 2, 2010, pp. 123–136.
4. Katsuhiko SAITO and Kiyohide HASEGAWA, 2008. *Foundation and Applications of Transport Package*. Japan, PA: Saiwaishobo, Inc.
5. Katsuhiko SAITO and Kazuaki KAWAGUCHI, Equivalent Drop Theory with Damping, *23rd International Association of Packaging Research Institutes Symposium*. 3–5 September 2007.
6. JIS-Z-0119-2002, *Mechanical-shock fragility testing methods for packaging and products design*.
7. ISO-8568-1989, *Mechanical shock—Testing machines—Characteristics and performance*.

Life Cycle Inventory Comparison of Paper and Plastic Based Packaging Systems for Strawberry Distribution

JAY SINGH* and ARIC KRASOWSKI

Packaging Program, Cal Poly State University, San Luis Obispo, CA

ABSTRACT: The goal of this study was to conduct a Life Cycle Inventory (LCI) analysis based comparison of eleven primary container and pillow wrap combinations for the distribution of fresh strawberries. Three of the primary containers studied were paper based (molded pulp, paperboard and corrugated fiberboard) and three other containers investigated were clamshells or punnets made of polyethylene terephthalate (PET) and recycled PET (rPET). Pillow wraps made of rPET and polylactide (PLA) were also included for all punnet/tray style containers. The scope of the study ranged from the extraction of raw materials, their processing and formation for all packaging components, product filling and distribution followed by their end-of-life scenarios. The scope includes energy inputs/credits and greenhouse gases in CO₂ equivalents followed by the end-of-life disposal. The functional unit selected was 0.45 kg of packaged strawberries delivered to institutional customers (on-site users) and retailers within 402 kilometers from the processing and packing plant with a minimum of one week of shelf life at delivery. When compared to the traditional PET clamshell style containers, the ten alternative packaging systems provide better energy usage/credit and GHG results. Molded pulp trays outperformed all alternatives studied in this regard, while the paperboard and corrugated fiberboard systems provide very practical and environmentally feasible alternatives. Scenario I for the end-of-life, which reflects a close approximation of the MSW treatment rates in the US, the paperboard and corrugated fiberboard based systems had a 3–4% and 12–17% improved performance towards the energy usage/credit and GHG emissions respectively.

1.0 INTRODUCTION

FRESH strawberries rank amongst the most perishable fresh fruits. Unlike most other fruits, strawberries are harvested and packed in a fully ripened state in the field. Due to their high susceptibility to

*Author to whom correspondence should be addressed. E-mail: jasingh@calpoly.edu

water loss and mechanical damage, they require special attention to all aspects of postharvest handling [1]. Immediately upon harvesting, strawberries are often packed in the retail packages (plastic clamshells, baskets, etc.), accumulated in “flats” or trays (plastic or corrugated) and palletized for cold chain distribution. Maintaining the temperature of this fruit between 0–1°C, while in staging for cooling, storage at cooler, distribution through refrigerated trucks as well as stocking for display at retail, is important to prolong its shelf life [1].

Strawberry production has been on the rise over the past two decades with approximately 36% increase between 1990 and 2007 and a global production of 3.82 million metric tons in 2007 [2]. California is the leading producer of fresh strawberries in the US, with over 88% of all shipments followed by Florida with approximately 11% [2]. Figure 1 shows the top ten countries in relation to strawberry production for 2007.

This study aimed at evaluating and comparing the manufacturing, product filling and distribution related environmental impacts of eleven primary container and pillow wrap combinations for the distribution of fresh strawberries. Three of the primary containers studied were paper based (fiber pulp, paperboard and corrugated fiberboard) and three other containers investigated were clamshells or punnets made of polyethylene terephthalate (PET) and recycled PET (rPET). The pillow wraps studied were made of rPET and Polylactide (PLA). A life cycle inventory (LCI) analysis was conducted for comparing the environmental outputs of these containers. LCI quantifies material use, energy use, environmental discharges, and wastes associated with each stage of a

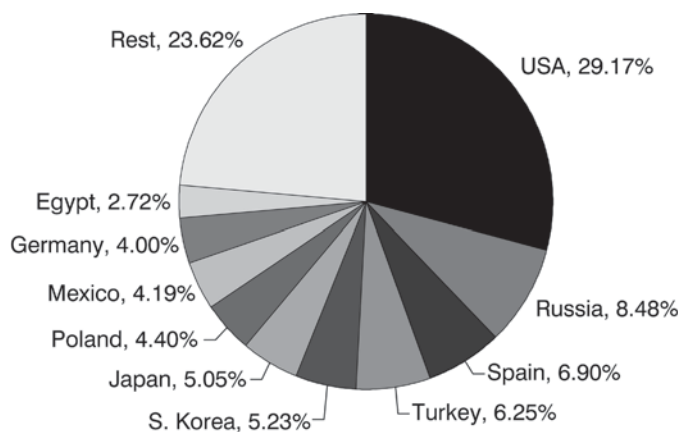


Figure 1. World Strawberry Production, 2007 [2].

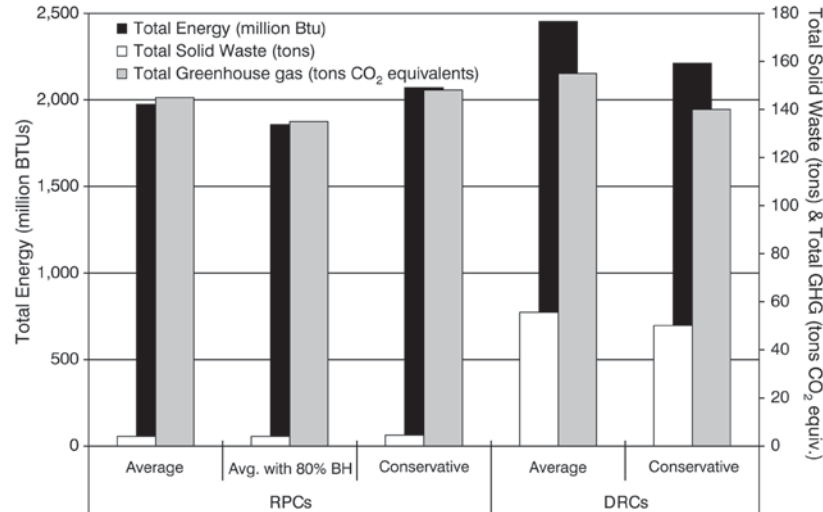


Figure 2. Summary of LCI Results for RPC and DRC Scenarios (for 1000 tons of strawberries shipped) [4].

product system over its life cycle, from raw material extraction through material processing, product fabrication, use, reuse or recycling, and ultimate disposal [3].

Very few past studies have researched the environmental issues related to packaging for strawberries. An LCI analysis study compared reusable plastic containers (RPC) to single-use display ready paper corrugated trays (DRC) for packing and shipping of ten categories of fresh fruits and vegetables. Based on the scope of the study, it was reported that overall the RPCs required 39% less energy, produced 95% less total solid waste and generated 29% lesser green house gases (GHG) [4]. Figure 2 shows the energy, solid waste and GHG results for the distribution of strawberries for the two types of containers. The average values reported for DRCs were based on the reported weights of the folded boxes and those for RPCs were based on the average reuse and loss rates reported. The conservative scenario for RPCs involves 75% of average reuse rate, twice the average loss rate and maximum backhaul distance and that for DRCs includes 10% lightweighting. Results for RPCs were also reported assuming a 20% reduction in backhaul distance of empty containers.

Several other studies have focused on the environmental impacts of cultivation and transportation of strawberries. It is estimated by one that, on a broad level, approximately 50% of food GHGs are emitted during the agriculture stage, with the remaining GHGs associated with

the phases after farming [5]. A study looked at the carbon footprint as part of a life cycle assessment (LCA) of strawberries grown in Spain for consumption in Western Europe, using Germany as an example. Using a 500 gram fresh strawberry PET punnet as the functional unit, the study accounted for the three most common GHGs emitted from agricultural activities—carbon dioxide (CO₂), nitrous oxide (N₂O) and methane (CH₄). The findings concluded that the largest part of the carbon footprint was attributed to transportation to consumer and packhouse (205 g CO₂ eq.) and consumer shopping (65 g CO₂ eq.) and strawberry cultivation (60 g CO₂ eq.) while agrochemicals (40 g CO₂ eq.) played a minor role [6].

A different research conducted a comparative study of the CO₂ emissions associated with fresh vegetables and fruits produced locally in Austria versus imported. Among the five products included in this study, strawberries imported from Spain and those grown domestically in Lower Austria were evaluated. The scope of this project was based on the transport associated emissions related to road, sea and air distribution. The CO₂ emissions for the domestic strawberries (6.9 g CO₂ eq.) were found to be approximately 3% as compared to those associated with the Spanish imports (264.4 g CO₂ eq.) [7].

A similar study as above was conducted in Spain to evaluate the energy saved and emissions avoided due to sourcing of fruits and vegetables from local farmers (within 200 km radius) rather than distant sources. Long stem strawberries did not have any impact due to unavailable local climate for their cultivation and these numbers were reported as 169 tons of oil equivalent and 425 tons of CO₂ equivalents for the energy and emissions respectively [8].

2.0 GOAL, SCOPE AND BOUNDARIES

2.1 Goal, Scope and Functional Unit

The goal of this study was to conduct an LCI analysis based comparison of eleven primary container and pillow wrap combinations for the distribution of fresh strawberries. Three of the primary containers studied were paper based (molded pulp, paperboard and corrugated fiberboard) and three other containers investigated were clamshells or punnets made of PET and rPET (Figure 3). Pillow wraps made of rPET and PLA were also included for all punnet/tray style containers. The scope of the study ranged from the extraction of raw materials, their process-

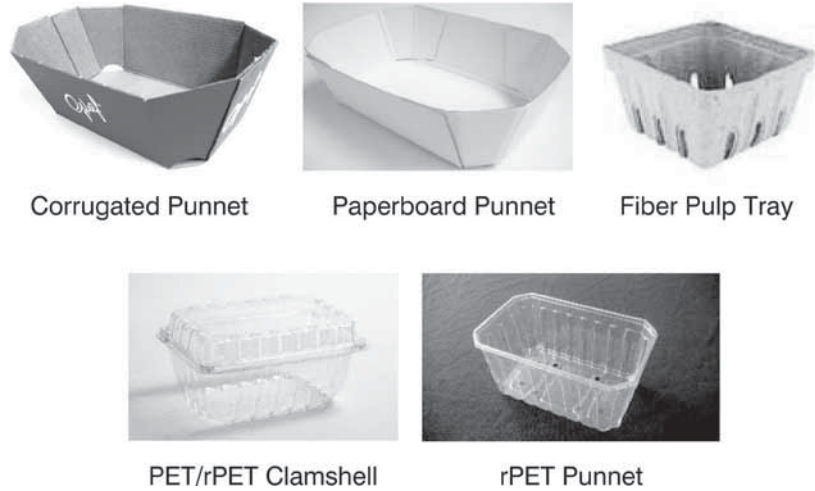


Figure 3. Primary Packages Studied.

ing and formation for all packaging components, product filling and distribution followed by their end-of-life scenarios. The scope includes energy inputs and credits and greenhouses gases in CO₂ equivalents followed by the end-of-life disposal. The functional unit selected was 0.45 kg of packaged strawberries delivered to institutional customers (on-site users) and retailers within 402 kilometers from the processing and packing plant with a minimum of one week of shelf life at delivery.

Figure 4 shows two of these containers with the strawberries. While the PET/rPET clamshells do not require any more packaging, the rPET and paper based punnets were assumed wrapped in rPET or PLA film “pillow”. The paperboard and corrugated fiberboard punnets provide a large “billboard”, for promoting the product carried within, at retail. This study investigated display ready corrugated containers (DRCs) as the transportation unit (Figure 5).



Figure 4. Packed Punnet and Clamshell Style Container Examples.



Figure 5. Display Ready Corrugated Shipper.

2.2 Methods

The framework of this study was adopted from ISO 14040 guidelines [1]. SavvyPack[®] 2.0 software system (Allied Development Corp., Burnsville, MN, USA), an LCI software program, and CAPE PACK v2.04 (Cape Systems Group, Inc., Piscataway, NJ, USA) pallet optimization software were used for this study. The SavvyPack[®] system measures energy usage and recovery and GHG emissions (CO₂ equivalent), through each step of the supply chain, including resin and other raw material production, raw material transport, package manufacture, product filling, and delivery to the retailers or institutional customers. The “United States 3” data set option offered by the LCI software was selected for this study. This data set is based on production processes in the United States and includes biomass energy credits. The CAPE PACK design software consists of pallet pattern optimization tools. Its features include the ability to build pallet patterns, create new case sizes, design new product packages and consolidate case sizes.

The raw material data required for the inventory analysis for the following was obtained from the SavvyPack[®] software: PET/rPET (clamshells/punnet); paper fiber pulp, paperboard and corrugated fiberboard (punnets); corrugated fiberboard (DRCs); rPET and PLA film (pillows); band straps (PET) and wood (pallets). This software sources the data and keeps it updated to within three months from the Canadian Raw Materials Database, European Aluminum Association, European Commission, Finnish Environment Institute, International Iron and Steel Institute, National Renewable Energy Lab, Environmental Defense Fund Paper Calculator, Plastics Europe, and Sustainable Product Information Network for the Environment.

A scorecard methodology to provide a comparison between the three

packaging systems studied was also incorporated in this study. This is particularly beneficial to all suppliers and retailers that are presently using scorecards to judge packaged products in terms of different metrics of sustainability. A scorecard may be construed as a document reflecting, in summary form, the strategic objectives, measures, performance targets and any explanatory narrative. Wal-Mart's packaging scorecard was introduced in the US in 2006 as a measurement tool that allows suppliers to evaluate themselves relative to other suppliers, based on specific metrics [9]. In the packaging scorecard system, the suppliers are required to enter information regarding the packaging of each product supplied to Wal-Mart. Each product packaging is then judged in terms of different metrics of sustainability that include GHG emissions produced per ton of packaging, size of packaging, use of raw materials, use of renewable energy, recycled content, transportation impacts, innovation, etc [9].

SavvyPack[®] software allows users to create a similar scorecard where the inbuilt matrices are populated during data input for the LCI analysis. The scorecard results for the eleven packaging systems studied were created with the following matrices and the weighted average for each based closely to that utilized by Wal-Mart:

- 15% based on Purchased Material GHG
- 15% based on Sustainable Material
- 15% based on Package to Product Ratio
- 15% based on Cube Utilization
- 10% based on Transportation Distance
- 10% based on Recycled Content
- 10% based on Recovery
- 5% based on Renewable Energy
- 5% based on Energy Innovation

This scorecard provides valuable input to any supplier who may have to meet mandates by retailers and can allow them to compare different packaging options for any product category.

2.3 Allocation

According to ISO 14040, allocation is defined as partitioning the input or output flows of a unit process to the product system under study [3]. During the performance of LCA, allocation may be necessary when

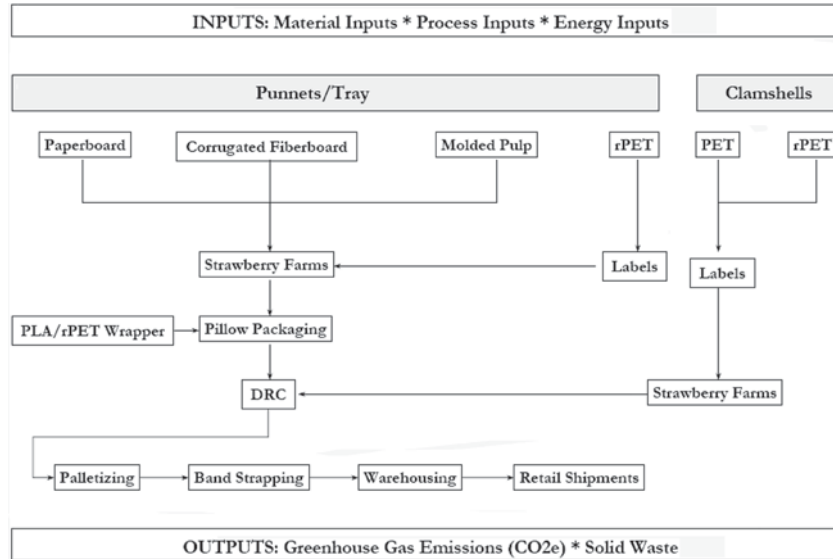


Figure 6. System Boundaries of Evaluated Systems.

a process yields more than one product i.e. a multifunctional process [10]. This study focused primarily on the fresh strawberry related package manufacturing, product filling, unitizing and distribution components as related to the six primary containers (and pillow wraps where applicable) as well as the distribution packaging involved. Strawberry production, harvesting and packing was excluded in this study. Allocation was not used in this study since there was no more than one input or output in each unit process.

2.4 System Boundaries

The system boundaries are illustrated in Figure 6. Strawberry production, harvesting and packing were not included in this study. It was assumed that any loss of product was the same for all eleven packaging systems studied. GHG in CO₂ equivalents and energies were analyzed based on materials (used to manufacture the packaging components, packaging of the product and the secondary packaging), processes (production facility and manufacturing processes for packaging components and packaging of the product) and transportation (raw materials, raw material packaging, finished product packaging from their point of origin to the production facility and transporting the finished product packaging from the production facility to the customer).

2.4.1 Primary Packaging

The primary package designs studied are shown in Figures 3 and 4 and contain three paper based (molded pulp, paperboard and corrugated fiberboard) and three plastic clamshells or punnet (PET and rPET). While the three plastic clamshells/punnets and the molded pulp trays are presently used widely in the U.S., the paperboard and corrugated fiberboard punnets are not. The latter forms of soft fruit containers are popular in Europe and in contrast to the other containers, provide a larger billboard for graphics. The different overall weights of the primary packages are provided in Table 1.

2.4.2 Secondary (Distribution) Packaging

As shown in the system boundary (Figure 5), the secondary packaging used for this study was primarily corrugated fiberboard DRCs, PET band straps and reusable wooden pallets. Table 1 provides details of the palletizing configurations for all eleven packaging systems studied. The palletizing configurations were based on the existing or recommended methodologies.

3.0 DATA AND DATA QUALITY REQUIREMENTS

3.1 Production of Raw Materials

The LCI data for production of all raw materials namely, PET and rPET (clamshells, punnet, pillow wrap and band straps), paper based substrates (molded pulp, paperboard and corrugated fiberboard), PLA (pillow wraps) and wood (pallets) was obtained from the SavvyPack[®] software. Details of the databases sourced by this software are provided in section 2.2. The following post consumer recycled content values were adopted for the raw materials used in all packaging systems: corrugated fiberboard, paperboard and pulped fiber (punnets and trays)—76.6%, PET (band straps)—27.2%, PET (clamshells)—0%, rPET (clamshells, punnets and pillow wraps)—50%, PLA (pillow wraps)—0% and wood (pallets)—14.8% [11].

3.2 Production of Packaging Components

The cradle-to-gate energy consumed or credited and CO₂ equiva-

Table 1. Packaging Design Differences for the 0.45 kg Strawberry Packaging Systems.

	PET Clamshell	rPET Clamshell	rPET Punnet/ RPET	rPET Punnet/ PLA	Paperboard Punnet/ rPET	Paperboard Punnet/ PLA	Molded Pulp Tray/rPET	Molded Pulp Tray/PLA	Corrugated Punnet/ rPET	Corrugated Punnet/ PLA
Weight of PET (kg)	0.027	N/A	N/A	N/A	N/A	N/A	N/A	N/A	N/A	N/A
Weight of rPET (kg)	N/A	0.027	0.025	0.025	N/A	N/A	N/A	N/A	N/A	N/A
Weight of paper based material (kg)	N/A	N/A	N/A	N/A	0.040	0.040	0.040	0.040	0.032	0.032
Weight of wrapper (kg)	N/A	N/A	0.003	0.003	0.003	0.003	0.003	0.003	0.003	0.003
Secondary packaging	DRC	DRC	DRC	DRC	DRC	DRC	DRC	DRC	DRC	DRC
Containers per pallet	840	840	840	840	840	840	840	840	840	840
Total weight of palletized load (kg)	574	574	675	675	762	762	804	804	776	776
Product weight per pallet (kg)	381	381	381	381	381	381	381	381	381	381
Packaging weight per pallet (kg)	193	193	294	294	381	381	423	423	395	395
Number of pallets per truck (kg)	22	22	22	22	22	22	22	22	22	22
Product weight per truck (kg)	8382	8382	8382	8382	8382	8382	8382	8382	8382	8382
Packaging weight per truck (kg)	4246	4246	6468	6468	8382	8382	9306	9306	8690	8690
Total weight per truck (kg)	12628	12628	14850	14850	16764	16764	17688	17688	17072	17072

lents generated to produce all packaging system components as well as associated with the disposal were available from the LCI software database. All plastic sheets/films were assumed manufactured using the extrusion process and the clamshells and punnet were thermoformed.

3.3 Consumption Stage

The filling of primary containers with freshly harvested strawberries was assumed identical for all eleven packaging systems and was excluded from this study. Unitization and storage prior to and during distribution of filled containers to institutional customers (on-site users) and retailers within 402 kilometers from the processing and packing plant were assumed to result in similar impacts. Automated cartoners, case packers, pillow form-fill-seal packers for all punnets and palletizers were included in this study. The details of the packaging configurations for all packaging systems are provided in Table 1. The pallet dimensions were assumed to be 102 cm × 122 cm × 15 cm and the truck dimensions were 2.4 m × 16.2 m × 2.8 m with a weight capacity of 19800 kg. Wooden pallets were assumed to have a useful life of 30 trips [4].

3.4 Distances and Transportation

Distance from all resin (PET, rPET and PLA) suppliers to the manufacturing centers averaged at 4828 km and included truck and train as the modes of transport. The labels were assumed to be shipped from 520 km to the primary packaging manufacturing sites. All finished packaging components including paper based packages, wooden pallets and PET band straps were assumed to be shipped to the farms from an average of 402 km. The overall cradle-to-gate energy and GHG ratios that converted energy use and GHG emissions to cradle equivalents for the truck and railcar transportation were available through the SavvyPack® LCI software.

3.5 End-of-Life

The following end-of-life scenarios in terms of landfill, incineration and recycling for all packaging components used in the eleven systems studied were considered. Both scenarios assumed that no packaging

was being retained by the institutional and retail customers and that all packaging materials underwent the waste treatment process.

- Scenario I—(40R/30I/30L)—40% recycling/30% Incineration/30% landfill
- Scenario II—(50I/50L)—50% incineration/50% landfill

Scenario I is close to the municipal solid waste treatment rates in the U.S. when observed across all materials used in the eleven systems studied [11]. Growing climate, energy and environmental concerns coupled with technological developments and regulatory changes have triggered a renewed interest in MSW as an energy source with the potential to provide renewable energy while reducing GHG emissions and the need for landfill space [12]. MSW-to-energy technologies being employed today include landfill gas capture (biogas made of approximately 50% CO₂ and 50% methane) [13], combustion (burning waste at approximately 980°C) [14], pyrolysis (MSW heated in absence of oxygen at approximately 290–700°C) [15], gasification (MSW heated with small amount of oxygen at 390–1650°C) [16] and plasma arc gasification (superheated plasma technology used to gasify MSW at approximately 5540°C) [17]. Landfill gas capture has achieved the widest acceptance amongst these technologies with bio-energy programs in place at 485 landfills in U.S. in December 2008 [18]. Waste combustion has not grown in acceptance since 1996 and presently there are 88 waste-to-energy plants in operation in 25 states [19]. Gasification and plasma arc technologies are still facing challenges towards commercial scale use [19]. Considering the increasing impact of landfill and incineration technologies, Scenario II was used in this study.

4.0 RESULTS

The main purpose of this study was to provide a relatively simple methodology to serve as a decision making tool when more than one packaging solution could be available to a user. For this reason, we provide environmental emissions of the packaging systems studied (LCI) and not the burdens (LCA). A full LCA needs to be undertaken to understand the impacts of the environmental burdens. Also due to recent mandates from retailers that use scorecards to judge packaged products in terms of different metrics of sustainability, this study incorporated it as a technique for comparing the eleven packaging systems studied.

Table 2. Greenhouse Gases and Energy Consumption.

Container/Wrapper	Energy (MJ/FU)		GHG (kg CO ₂ eq/FU)	
	40R/30I/30L	50I/50L	40R/30I/30L	50I/50L
PET Clamshell/(N/A)	102.77	96.62	6.95	7.37
RPET Clamshell/(N/A)	99.09	91.17	6.35	6.90
RPET Punnet/RPET	91.06	84.99	5.86	6.29
RPET Punnet/PLA	89.99	83.92	5.84	6.27
Paperboard Punnet/ RPET	98.66	97.45	5.92	6.01
Paperboard Punnet / PLA	99.04	97.83	6.14	6.22
Molded Paper Tray/RPET	97.79	96.58	4.18	4.27
Molded Paper Tray/PLA	96.71	95.51	4.16	4.25
Corrugated Punnet/RPET	99.76	98.55	6.19	6.27
Corrugated Punnet/PLA	99.04	97.83	6.14	6.22

4.1 Discussion

Based on the data collected, GHG output (kg CO₂ eq) and energy use/credit (MJ) per functional unit, and the scorecard results from the analysis were tabulated. Table 2 and Figures 6 and 7 show the GHG output and energy uses for the two end-of-life scenarios considered. Table 3 shows the results in a scorecard format.

4.1.1 Energy Usage Results

The energy use/credit was studied for the eleven 0.45 kg strawberry packaging systems. Figure 7 shows the percentage difference in

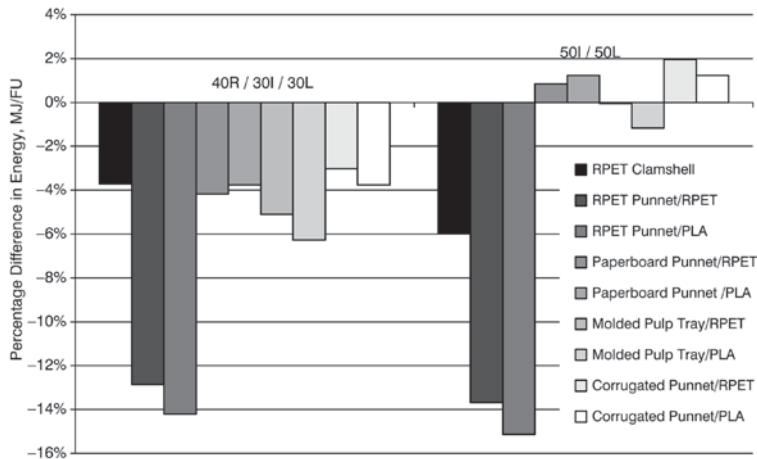


Figure 7. Percentage Difference in Energy Usage Compared to PET Clamshell.

Table 3. Packaging Scorecard Results.

Criterion	Max Score	PET		rPET		Paperboard		rPET		Paperboard		Molded Pulp		Molded Pulp		Corrugated	
		Clamshell	Punnet/ PLA	Clamshell	Punnet/ PLA	rPET	Punnet/ PLA	Punnet/ rPET	PLA	Punnet/ rPET	Punnet/ PLA	Tray/rPET	Tray/PLA	rPET	Punnet/ rPET	Punnet/ PLA	
Purchased Material GHG	15	10.36	12.38	10.85	12.38	14.33	14.33	12.38	14.33	14.33	14.33	14.33	10.85	10.85	10.85	10.85	
Sustainable Material	15	6.61	13.62	6.61	13.62	12.11	12.11	13.62	12.11	12.11	12.11	12.11	6.61	6.61	6.61	6.61	
Transportation Distance	10	4.39	9.08	4.39	9.08	10.00	10.00	9.08	10.00	10.00	10.00	10.00	4.39	4.39	4.39	4.39	
Package to Product Ratio	15	6.05	12.80	6.05	12.80	12.80	12.80	12.80	12.80	12.80	12.80	12.80	6.05	6.05	6.05	6.05	
Cube Utilization	15	7.50	7.50	7.50	7.50	7.50	7.50	7.50	7.50	7.50	7.50	7.50	7.50	7.50	7.50	7.50	
Recycled Content	10	7.10	10.00	6.45	10.00	9.08	9.08	10.00	10.00	9.03	9.03	9.03	6.45	6.45	6.45	6.45	
Recovery	10	6.22	7.98	6.55	7.98	8.48	8.48	7.97	8.48	8.46	8.46	8.46	6.55	6.55	6.55	6.55	
Renewable Energy	5	2.50	2.50	2.50	2.50	2.50	2.50	2.50	2.50	2.50	2.50	2.50	2.50	2.50	2.50	2.50	
Energy Innovation	5	2.50	2.50	2.50	2.50	2.50	2.50	2.50	2.50	2.50	2.50	2.50	2.50	2.50	2.50	2.50	
Total	100	53.23	78.36	53.40	78.35	79.25	79.25	79.25	79.25	79.23	79.25	79.23	53.39	53.39	53.37	53.37	

energy usage for all systems studied in comparison to the PET clamshells. When compared to the traditional PET clamshells, all ten alternate packaging systems had lower energy usage for Scenario I. The RPET punnets wrapped in PLA or rPET pillows showed the lowest energy use with approximately 14% and 13% debit respectively in comparison to the PET clamshells. The paper based alternatives overall had a decreased energy usage in the range of approximately 3–6% by comparison. Scenario I reflects an approximate representation of the municipal solid waste treatment rates in the U.S. [18]. In Scenario II, the RPET punnets wrapped in PLA or rPET pillows showed the lowest energy use with approximately 14% and 13% respectively in comparison to the PET clamshells. All paper based alternatives were approximately at par.

4.1.2 Greenhouse Gas (CO₂e) Results

Figure 8 shows the percentage difference in GHG emissions (CO₂e) for all systems studied in comparison to the PET clamshells. It was observed that all alternate systems contributed significantly lower GHG emissions for both end-of-life scenarios when compared to the traditional PET clamshells. For Scenario I, while the rPET punnets wrapped in either PLA or rPET pillow had a reduced GHG emission of approximately 19%, the paperboard and corrugated fiberboard punnets had a

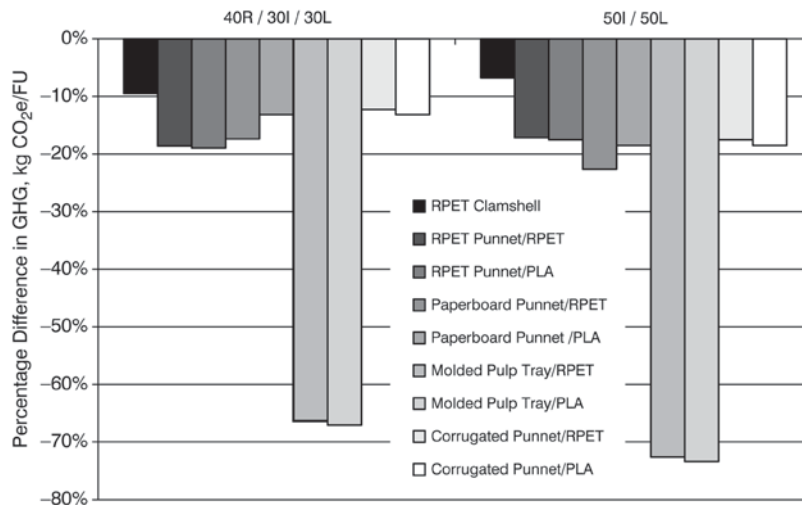


Figure 8. Percentage Difference in Greenhouse Gases (CO₂e) Compared to PET Clamshell.

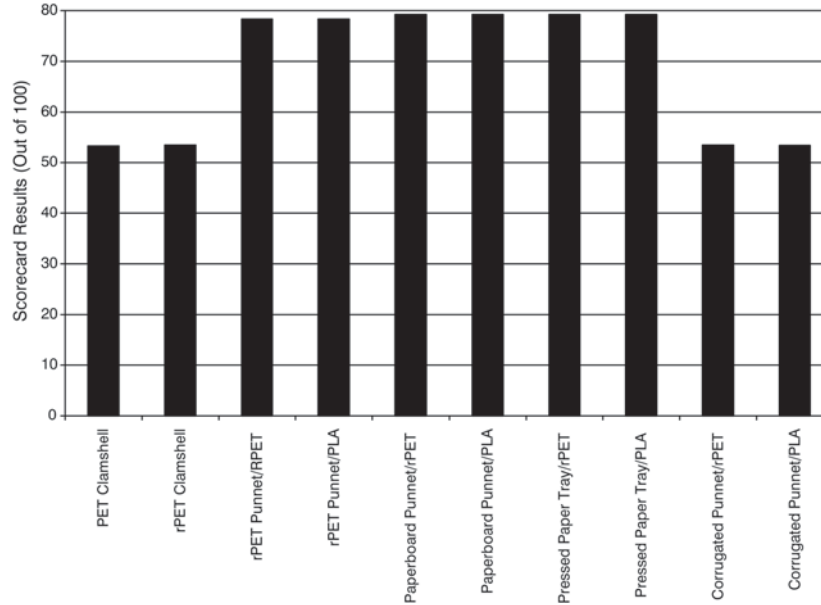


Figure 9. Overall Scorecard Results (100 Maximum).

debit ranging between 13–17%. The molded pulp trays had a dramatic reduction in GHG emissions of approximately 67% by comparison. For Scenario II, while the rPET punnets wrapped in either PLA or rPET pillow had a reduced GHG emission of approximately 17%, the paperboard and corrugated fiberboard punnets had a debit ranging between 18–23%. The molded pulp trays had a dramatic reduction in GHG emissions of approximately 73% by comparison.

4.1.3 Scorecard Results

Table 3 and Figure 9 show the results in the SavvyPack[®] scorecard format. It may be seen that when compared to the PET clamshells, the rPET clamshell and both corrugated fiberboard systems were only slightly better. The rPET punnet, paperboard punnet and molded pulp trays, on the other hand, scored 47–49% higher by comparison.

5.0 CONCLUSIONS

The main purpose of this study was to provide a relatively uncomplicated methodology to serve as a decision making tool when more than one packaging solution is available to a user. It conducted a LCI analy-

sis, and as related to a complete LCA study, the outcomes are limited. A full LCA needs to be undertaken to understand the impacts of the environmental burdens. Through the investigation of the eleven packaging systems in this study, it was shown that several viable material and packaging options exist for fresh strawberry distribution. It was also shown that using LCI and scorecards as tools for “sustainable” package design can be accomplished and can assist in uncovering overlooked aspects of a packaging system.

While the three plastic clamshells/punnets and the molded pulp trays are presently used widely in the US, the paperboard and corrugated fiberboard punnets are not very popular yet. The latter forms of soft fruit containers are popular in Europe and in contrast to the other containers, provide a larger billboard for graphics. It may be noted here that the plastic based clamshells or punnets typically are decorated using labels and the molded pulp trays typically do not get decorated. The advantage of paperboard or corrugated fiberboard punnets is the integrated decoration in the form of on-package printing achievable using a traditional container forming process such as flexo-folding-gluing.

When compared to the traditional PET clamshell style containers, the ten alternative packaging systems provide better energy usage/credit and GHG results. Molded pulp trays outperform all alternates studied in this regard, while the paperboard and corrugated fiberboard systems provide very practical and environmentally feasible alternatives. Scenario I for the end-of-life, which reflects a close approximation of the MSW treatment rates in the U.S., the paperboard and corrugated fiberboard based systems had a 3–4% and 12–17% improved performance towards the energy usage/credit and GHG emissions respectively.

As shown through the scorecard results, it may be seen that when compared to the traditional PET clamshells, the rPET clamshells and both corrugated fiberboard systems were slightly better. The rPET punnet, paperboard punnet and molded pulp trays, on the other hand, scored 47–49% higher by comparison. This information would be very beneficial to organizations who must comply with these kinds of recent mandates.

The optimum choice for the packaging systems for fresh strawberry distribution must rely on several issues. Some of these include any regulatory issues related to packaging materials in direct contact with food products, protection from distribution related hazards including the ambient and physical abuse, cost, environmental impacts and performance on scorecard type grading systems.

ACKNOWLEDGEMENT

The authors would like to acknowledge the support and funding provided by the Consortium for Packaging Technology and Science at California Polytechnic State University as well as Allied Development Corporation in making this research possible.

REFERENCES

1. California Strawberry Commission. Best Handling Practices for Strawberries. www.calstrawberry.com, accessed November 23, 2009.
2. United State Department of Agriculture. Economics, Statistics and Market Information System, U.S. Strawberry Industry (95003). Available at <http://usda.mannlib.cornell.edu/MannUsda/viewDocumentInfo.do?documentID=1381>, accessed November 24, 2009.
3. ISO 14040 (2006): Environmental management—life cycle assessment—principles and framework. ISO 14040:2006.
4. Singh SP, Chonhenchob V, Singh J. Life cycle inventory and analysis of re-usable plastic containers and display-ready corrugated containers used for packaging fresh fruits and vegetables. *Packaging Technology and Science*, 2006; 19: 279–293.
5. Elbourne, P. Reducing food-related greenhouse gas emissions through local production of fruit and vegetables. A report for Alness Town Transition Group, UK, July 2009. Available at http://www.communitypowerdown.org.uk/userfiles/file/documents/Deliverables%5CLocal_Food_Production/Peter%20Elbourne%20-%20Local%20Food%20Production%20GHG%20Savings.pdf, accessed November 25, 2009.
6. Blanke, M. Life cycle analysis and carbon footprint of imported Huelva Strawberries. Life Cycle Assessment IX Conference Proceedings, Boston, Massachusetts, September 29–October 2, 2009.
7. Annual Report, 2007. Calculation of the CO₂ rucksacks of imported versus regionally produced goods. Sustainable Europe Research Institute (SERI), Garnisonsgasse 7/27, 1090 Vienna, Austria.
8. Aranda, A., Scarpellini, S., Zabalza, I. and Valero Capilla, A. An analysis of the present food's transport model based on a case study carried out in Spain. *Proceedings of the 6th Int. Conf. on LCA in the Agri-Food Sector, Zurich*, November 12–14, 2008. pp 332–414.
9. Wal-Mart Press Release. November 1, 2006. Wal-Mart Unveils “Packaging Scorecard” to Suppliers. <http://walmartstores.com/pressroom/news/6039.aspx>. Accessed February 20, 2010.
10. Eide, M. H. Life Cycle Assessment (LCA) of Industrial Milk Production, *Int. J. LCA*, 7 (2), 115–126 (2002).
11. U. S. Environmental Protection Agency (2009) Municipal Solid Waste Generation, Recycling, and Disposal in the United States: Facts and Figures 2008.
12. Environmental and Energy Study Institute. Reconsidering Municipal Solid Waste as a Renewable Energy Feedstock. Issue Brief July 2009.
13. Environmental Protection Agency. LFG Energy Project Development Handbook, Chapter 1. Environmental Protection Agency, http://www.epa.gov/lmop/res/pdf/pdh_chapter1.pdf, 2009. Accessed May 18, 2010.
14. Hazardous Waste Resource Center. Hazardous Waste Incineration: Advanced Technology to Protect the Environment. Environmental Technology Center, <http://www.etc.org/technologicalandenvironmentalissues/treatmenttechnologies/incineration/>, 2000. Accessed May 18, 2010.
15. Kai Sipilä, Municipal and Commercial Solid Waste for Pyrolysis (Oils) and Gasification Markets. VTT Processes, <http://www.pyne.co.uk/docs/488.pdf>, 2002. Accessed May 18, 2010.
16. Zafar, S. Gasification of Municipal Solid Waste. Earthtoys Magazine, http://www.earthtoys.com/emagazine.php?issue_number=09.06.01&article=zafar, 2009. Accessed May 18, 2010.

17. Westinghouse Plasma Corporation. What is Plasma & Gasification? Westinghouse Plasma Corporation, http://www.westinghouse-plasma.com/technology_solutions/what_is_plasma_gasification.php, 2007. Accessed May 18, 2010.
18. Psomopoulos, C.S., A. Bourka, and N.J. Themelis. Waste to Energy: A Review of the Status and Benefits in the United States. Waste Management, <http://www.nmwda.org/news/documents/Tab3-Psomopoulosetal2009WTEstatusandbenefits2.pdf>, 2009. Accessed May 18, 2010.
19. Ramsey/Washington County Resource Recovery Project. Updated Research Study: Gasification, Plasma, Ethanol, and Anaerobic Digestion Waste Processing Technologies. Foth Infrastructure and Environment, LLC. Project I.D.: 07R001, May 2008.

The Effect of Moisture Content on Compression Strength of Boxes Made of Solid Fiberboard with Polyethylene Coating—An Experimental Study

SARA PAUNONEN* and ØYVIND GREGERSEN

Norwegian University of Science and Technology NTNU, Department of Chemical Engineering, Høgskoleringen 6B (PFI building), NO-7491 Trondheim, Norway

ABSTRACT: Factory-made transport boxes made from polyethylene coated solid fiberboard were studied. The boxes had double panel walls. Compression strength, vertical deformation, and buckling of long panels during top-to-bottom compression were studied for different moisture contents. The boxes were exposed to high humidity for eight days (90% RH; 4°C), and both standard BCT tests and cyclic load BCT tests were executed. During the BCT tests, buckling of the longest side was measured with linear transducers. The compression strength was observed to decrease linearly by 380 N per one percent change in moisture content. During eight days of exposure to a high humidity environment, the boxes lost 15% of their compression strength and gained 1 percent moisture content. The decrease of the BCT value relative to change in moisture is comparable to earlier results for uncoated corrugated boxes. The polyethylene coated boxes take longer to reach the moisture content change. Box failure can be expressed as a critical vertical displacement value that does not depend on the moisture content of the box. The boxes deformed mainly permanently during compression. The permanent deformation increased as a function of moisture content, and as a consequence the outward buckling of the vertical box decreased as the moisture content increased. Because of the polyethylene coating, the moisture was unevenly distributed in the boxes.

INTRODUCTION

THE main purpose of the transport box is to resist mechanical and to some extent environmental loadings so that the contents reach the final destination intact. The mechanical loadings include mechanical dynamic loading (e.g., accelerations from transport vehicle), static

*Author to whom correspondence should be addressed. E-mail: sara.paunonen@chemeng.ntnu.no

loading (dead weight of the stack) and hydrostatic loading (contents). The boxes undergo irreversible changes to their shape under the applied forces. During long term transportation and storage, the container also experiences time dependent phenomena typical for paper-based materials, e.g., creep. The ambient relative humidity and temperature affect the mechanical properties of boxes [1]. The usual and simplest way of quantifying a box's performance is to measure the maximum force applied in a box compression test (BCT) at standard conditions.

This work studies the effects of moisture on the performance of transport boxes that are made from polyethylene coated solid fiberboard. Boxes have an unusual, more complicated design compared to well-known regular slotted containers. The box testing is done at conditions close to the actual transport conditions of fresh round fish (constant 4°C and 90% RH). Creep of the boxes at constant RH is studied, but creep in varying humidity is left out since the conditions do not change during transport. The transport duration (eight days) is taken as the time frame of the experiments.

The objectives of the study are to

1. Quantify the moisture content and determine its impact on box compression strength,
2. Examine the deformation of boxes, and
3. Examine the outward buckling of the outer panel of a double-paneled box wall

BACKGROUND

Box Compression Test (BCT)

Single box compression has been used to simulate box performance in the end-use situation for a long time, even though a box cannot sustain the same stacking load obtained in a compression test [2],[3]. BCT tests have a large standard deviation in the results due to, variation in raw material, imperfections in the box geometry from the manufacturing process, and environmental conditions during the testing. The large standard deviation easily masks the effect of the variables studied. In a controlled test environment, the 2-sigma variation of BCT results of individual factory made boxes (same quality) over time is normally $\pm 14\%$, even as high as $\pm 20\%$ [4]. The same conditions that change the top-to-bottom compressive strength in the laboratory, also change the

amount of time that a box can support dead loads when stacked during transportation or in storage [5].

Compression strength of a container depends on the material properties of the paperboard layers, their geometric arrangement in the built-up board, the manufacturing process of the box (e.g., depth of scoring) [6], the geometry of the box, and the test environment. For corrugated fiberboard, the key parameter contributing to the box performance is the compressive strength of the liner [7]. For solid fiberboard, no such clear results exist. One can anticipate that the compression strength of all layers is of importance.

The box compression test measures how different structural parts of the box; panels, edge creases, possible flaps and flap creases, resist the total top-to-bottom compressive load. The geometry of the box, the allocation and position of board materials all affect the distribution of compressive stress in transport boxes [8]. The vertical edges of regular slotted containers (RSC) are reported to carry 40–64% [8,9] of the total load during compression. The remaining load is carried by the panels. Meng et al. [9] used a pressure sensitive film to detect the load distribution along the box perimeter. Different parts of the package contribute to the stiffness of the whole box. The stiffness of the middle section of a box is higher than of the top and bottom sections, where the behavior of the creases affect the compression stiffness [10,11].

In a compression test, a box is loaded from top to bottom between two plates, and the force is recorded as a function of vertical displacement (BCT curve). Due to the irregular shape and the lack of precision in dimensions of the box during converting, the plates of the box compression tester don't contact the perimeter of the box evenly at the beginning of the test. The effect is seen as a flat slope in the BCT curve. In BCT test standards, e.g., [12], the effect of this gradual build-up of the load is handled with a preload that is a function of the expected strength of the box. The measurement of deformation is considered to start from this point. As the compression proceeds, the horizontal scoreline regions start to take the load by both crushing and rotation [13]. The sidewall tube bears the same load, but since the stiffness of the sidewalls is greater than the stiffness of the scoreline areas, the deformation occurs mainly in the scoreline areas. The end of the scoreline crushing phase shows up as a change in slope in the BCT curve. For corrugated boxes, 90% of the total deformation at maximum load (measured from zero load) occurs in the creased areas [13].

Since the edges of the box experience the most stress, failure starts

at the box corners (regions where the length, width and depth meet) and progresses into the panels [8,13,14]. Visible lines appear at the corners, and they grow towards the centre of the panel, and ultimately cause the panels to buckle. For corrugated fiberboard, McKee and Gander [13] suspect that the failure is due to compressive failure of the fluted medium. The failure is seen as a rapid decrease in the BCT curve. For corrugated boxes, the failure mechanism can be attributed to the loss of transverse shear rigidity of the corrugated board [15]. Other possible mechanisms include local buckling of the liner or global buckling of the panel depending on the slenderness ratio of the panel [16]. No results are available on the failure mechanism of solid fiberboard materials in transport packages.

Marcondes [17] studied the effect of loading history on the compression strength of corrugated boxes. He loaded the boxes to 60% and 80% of the compression strength 1 to 20 times before loading to failure. He found out that preloading do not significantly alter the compression strength of corrugated boxes.

Moisture Effects on BCT

The moisture content affects the mechanical properties of paperboard materials [1] and thus the boxes made of paperboard [2]. Kellicut [18] found a negative exponential relationship between compression strength Y of corrugated boxes and their moisture content m ,

$$Y = b \cdot 10^{-mx} \quad (1)$$

where b = compressive strength of a box at zero moisture content, m = average slope of the curve where moisture is plotted against the logarithm of compressive strength, and x = dry-based moisture content (ratio between the weight of water in the board and oven-dry weight of the fiberboard). Kellicut [18] observed that the boxes made of different corrugated materials responded in a similar way to increases in moisture content, and thus the parameter m was found to have a value of 3.01.

The in-plane deformation of panels at collapse is independent of deformation rate, relative humidity and the magnitude of dead-load [19]. Hansson [19] derived this conclusion by studying corrugated panels under compression, which was considered to be a more controllable test set-up than compression of whole boxes. If extended to boxes, the vertical displacement at compression strength would be independent of moisture content of the box. The box failure criterion could be expressed as

$$u \geq u_c \quad (2)$$

where u = vertical displacement of the box, and u_c = critical vertical displacement independent of material moisture content.

Often the moisture content is considered as a global variable of the box. One reading can be taken as an average of a samples of several boxes [20]. Sometimes the relative humidity on both sides of the box wall are recorded [21]. The rate of the moisture penetration into the boxes or the local variation in the moisture content is usually not studied.

Creep

Compression tests are performed relatively quickly, and no attention is paid to the time-dependent characteristics of the material. In reality, box failure occurs slowly. Compressive creep failure is the main reason for the transport boxes to fail in service [22]. The creep effect is accelerated both in paperboard and corrugated boxes in environments where the humidity changes. This causes earlier failure than at constant humidity [23]. Even though mechano-sorptive effects occur with small moisture content changes [24], mechano-sorptive creep is left out of the study since both the temperature and the relative humidity are stable during the transport in an air-conditioned truck. In addition, the high grammage and the PE coating of solid fiberboard slow down the moisture transport, the hygroexpansion and creep response, and make measurements challenging. The environment during transportation is a constant 90–100% RH/4°C. Coffin [25] gives a comprehensive survey on creep behavior of paper at constant and varying humidity.

EXPERIMENTAL

Materials

The paperboard studied is a uni-directionally stacked solid fiberboard; see Table 1 for material properties. The four middle layers are made of 100% recycled fiber (OCC) and are heavily internally sized. The outer layers on both sides are made of bleached machine finished kraft paper. The kraft paper has a double extrusion coated low-density polyethylene layer. The six paper and board layers are glued together in an industrial lamination process that compresses the material. The

Table 1. Grammage and Thickness of the Solid Fiberboard and Its Layers.

	<i>Name of Layer</i>	<i>Grammage [g/m²]</i>	<i>Thickness(*) [mm]</i>
1	Polyethylene coating	20	0.02
2	Kraft paper 1	60	0.07
3	Adhesion layer 1	10	
4	Middle layer 1	250	0.39
5	Adhesion layer 2	10	
6	Middle layer 2	250	0.39
7	Adhesion layer 3	10	
8	Middle layer 3	250	0.39
9	Adhesion layer 4	10	
10	Middle layer 4	250	0.39
11	Adhesion layer 5	10	
12	Kraft paper 2	60	0.07
13	Polyethylene coating	20	0.02
	Solid fiberboard	1220	1.73

glue used in lamination contains poly-vinyl alcohol (PVA) as an active agent, clay, additives, and water. The solids content of the liquid glue is 24%.

The design of the transport box is more complex than the commonly used regular slotted container (RSC) or similar boxes. The box has long walls that are made of two panels. The long inner panels are glued to the bottom panel. The short walls are made of single panels. The webbed corners prevent leakages and allow the vertical edges and short panels to buckle outwards when vertically loaded. Four small flaps hold the box structure together when glued onto the outer long wall panels. The outer dimensions of the transport boxes are 790 mm × 380 mm × 138 mm. The erected transport box is shown in Figure 1.

Box Compression Tests

Boxes with different moisture contents were exposed to a humid environment (90% RH, 4°C) for eight days. Before the trial, the boxes were stored at the test site at room (non-standard) temperature and relative humidity. Table 2 summarizes the different treatments. For Case B and C, boxes were pre-dried. The 3 liter water content was used to simulate the water present in the boxes during the transport.

After 24 hours (1 day), 96 hours (4 days) and 192 hours (8 days) three boxes from each case were taken from the climate room and box compression tested (BCT) at non-standard conditions (21–23°C,



Figure 1. The transport box design used in the study.

28–41% RH) with Alwetron CT100 (Lorentzen&Wettré) compression tester and Test&Motion (ICS) software according to the ISO standard 12048-2:1994 [12]. Throughout the work, empty boxes were tested, and the loose small flaps inside the box were taped onto the short panels. The rate of loading was 10 mm/min. The sampling frequency of the force-displacement data was 50 Hz. In the BCT test data analysis, the deformation is considered to start after a threshold value of 250 N. Table 2 also shows the reference cases (Ref, RefB, RefC) without the climate treatment.

Moisture content was measured at locations shown in Figure 2 by cutting two samples and drying them at 103°C for 3 days. Moisture content was also measured as weight increase in a whole box.

Deformation of Boxes

To study the deformation of the boxes more closely, a simplified version of the above mentioned test was executed. The treatments A and B shown in Table 2 were selected. Moisture and cyclic box compression were tested after 8 days of climate treatment. Reference boxes Ref and RefB were tested without the climate treatment. Six parallel boxes were compression tested cyclically with increasing loads (1000 N, 2000 N, 3000 N, ...). The box was loaded to the first load level, the load was removed and the compression plates were brought to the original posi-

Table 1. The Five Test Cases for Studying Liquid Water and Water Vapor Penetration into Fiberboard Boxes.

Test	Pretreatment		Box Content	Environmental Conditions	
	T [°C]	Time [d]		Climate [% RH/°C]	Time [d]
A	–	–	–	90/4	8
B	40	4	–	90/4	8
C	80	2	–	90/4	8
D	–	–	water (3 l)	90/4	8
E	–	–	water (3 l)	~ 50/23	8
REF	–	–	–	–	–
REFB	40	4	–	–	–
REFC	80	2	–	–	–

tion. Then the load was increased to the next force level, etc. Data from the unloading phase was not recorded.

In the creep test, a stack of three empty boxes was kept for eight days in a humid environment (90% RH, 4°C). The stack was loaded with a dead weight of 244 kg, which corresponds to 40% of the BCT value. The transport box at the bottom of the stack should be able to endure a dead-load of 260 kg. After eight days of exposure the creep tested boxes were BCT tested at room temperature.

Buckling of the Panels

The outward buckling of the long outer panel during the box compression test was measured with three linear displacement transducers (RDP Electronics LTD, type DCT1000A) that were mounted on a rack.

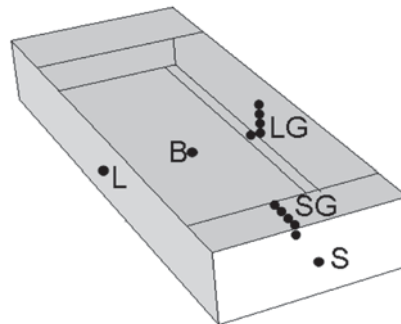


Figure 2. The locations for cutting material moisture samples: short panel (S), long panel (L), bottom panel (B), gradient measurement (five 20 mm long samples) from the short edge (SG), gradient measurement from the long sheet edge (LG). The length of the gradient measurement is 100 mm. The size of the material samples was approximately 20 mm × 20 mm.

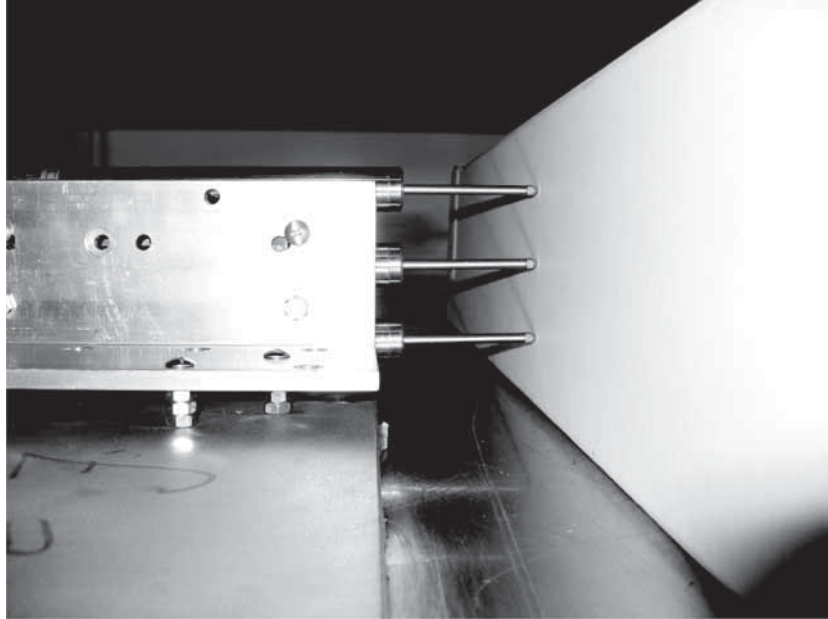


Figure 3. Three displacement transducers measuring the outward buckling of the long wall before the start of a BCT test.

The transducers were placed vertically in the middle of the long side of the box. The distance between the sensors and box edges was one quarter of the height of the box as seen in Figure 3. The transducers were connected via Contrec AQ-Box to a PC, and Contrec Winlog 2000 program was used for data acquisition at a sampling frequency of 50 Hz.

RESULTS AND DISCUSSION

Moisture Content of Boxes

Figure 4 shows the change in moisture content over 8 days when the boxes were pre-dried in 40°C before they were exposed to 90% RH and 4°C (test Case C). Moisture penetrates through the material edges and the moisture content increases gradually further and further away from the edges. The penetration through box side panels is relatively low. After eight days, only the first 100mm from the sheet edge is affected by moisture penetration. The overall moisture uptake of the boxes is measured by weighing the whole box as shown in Figure 5. The measured moisture increase of 1 percent is close to the increase of 0.5–1 percent reported by Kirkpatrick [26]. The values of Kirkpatrick are for

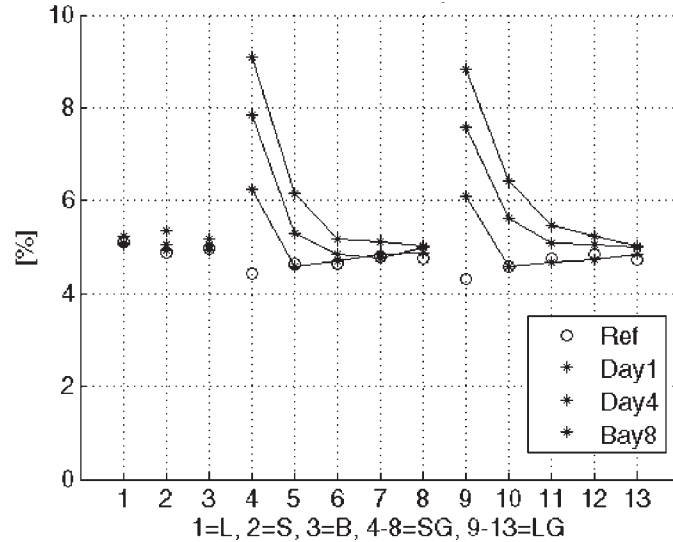


Figure 4. Development of moisture content at different locations of the box during climate treatment: short panel (S), long panel (L), bottom panel (B), gradient measurement from the short edge (SG), gradient measurement from the long sheet edge (LG). The location on the box is shown on the x-axis. Moisture contents are measured from samples taken in days 1, 4, and 8, average value ($n = 2$, $n =$ number of averaged data points).

a PE-coated corrugated fiberboard boxes measured at 20°C after 8 days cyclic (60%/90% RH) moisture treatment. In Cases D-E, the high variation in the moisture increase is due to the difficulty in drying the excess water before weighing. These cases are left out of further discussion.

The moisture content increase of a transport box due to humidity is often reported as the average increase in container weight [27], average value taken from several boxes [20], or as a relative humidity measurement taken from the outer and inner side of the material [27]. For corrugated boxes these techniques are justified because there is no additional moisture barrier slowing down the moisture sorption. There is no difference in the moisture transport rate in-plane and through-plane. Polyethylene coating slows down the transverse moisture transport considerably, and leads to uneven moisture distribution of the box. This effect was seen as there was relatively little moisture intake in the boxes during the climate treatment. A 100 mm wide strip near the open material edges has considerably higher moisture content than the middle of the box panels. The average moisture content of a box does not provide a reasonable basis for comparing the strength properties. Instead the moisture content of the load bearing parts should be used. However, the average moisture by weighing the whole box is a quick, reliable, and

non-intrusive measurement. In the following discussion this measurement description technique is used.

Impact of Moisture Content on Box Compression Strength

Figure 6 shows the box compression strength as a function of average moisture content. The original moisture content was defined as the average of the three measurements from the middle of the panels (Figure 3, locations L, S and B). The moisture increase is taken from the data presented in Figure 5. In Cases B and C, the moisture penetration of pre-dried boxes was measured. Ventilation conditions during the drying affect the moisture content. The boxes for Cases B and C and for the reference cases RefB and RefC (see Table 2) were dried in different batches, and thus the compression strength values in Figure 6 are only indicative.

The decrease of BCT values in Figure 6 is almost linear with respect to the moisture content, as also reported by Kellicut [18]. By omitting the reference, the compression strength decreases 380N per moisture content percent. The polyethylene coated solid fiberboard boxes lost 15% (from 5500N to 4700N) of their compressive strength by being exposed to high humidity in eight days. During that time, the moisture content increased by 1 percent. According to [28], corrugated containers

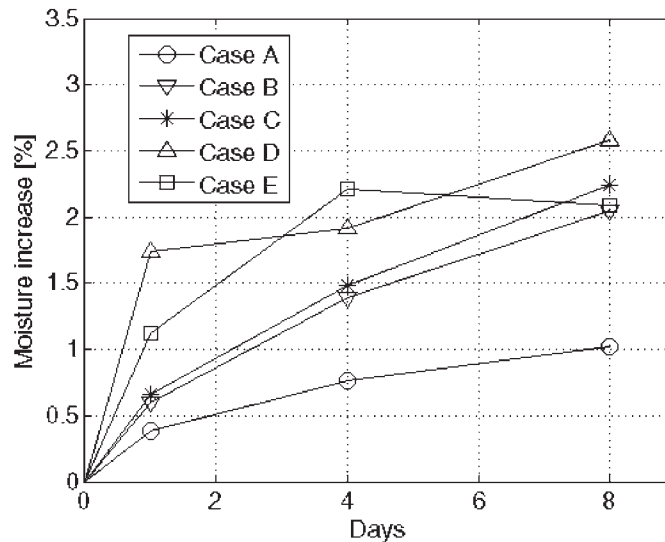


Figure 5. Moisture increase of boxes during climate treatment measured by weighing the whole box, average value (n = 3).

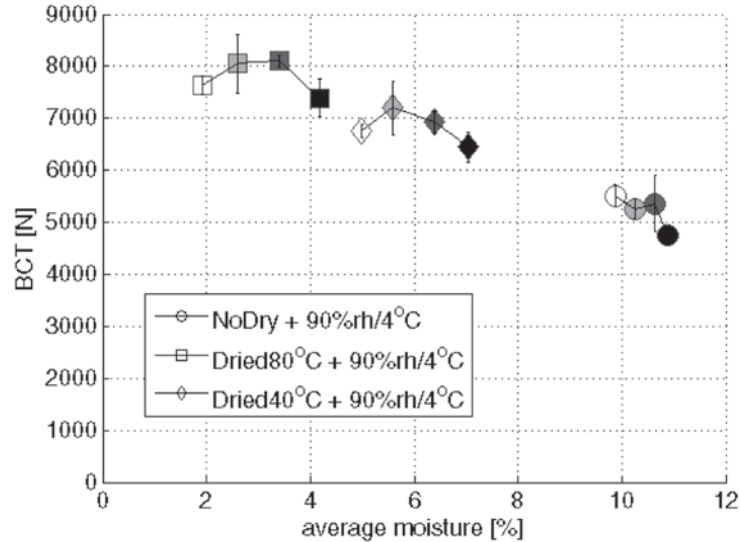


Figure 6. Box compression strength as a function of average moisture content. Marker types: 'O' = non-pretreated boxes (Case A), '◇' = pre-dried in 40°C (Case B), '□' = pre-dried in 80°C (Case C), Marker colors: white = references, gray = day 1, dark gray = day 4, black = day 8. Average and standard deviation ($n = 3$).

typically lose 10–20% of their compressive strength at 50% RH in high humidity environments. Data presented by Kellicut [18] shows that an increase in moisture content from 6% to 7% decreases the compression strength of uncoated corrugated boxes by 9%. An increase from 6% to 18% in moisture content would result in 56% reduction in compression strength. The decrease of 15% in compression strength for PE coated boxes is in line with the results by Kellicut [18], keeping in mind the moisture barrier role of the polyethylene. The results seem to hold even for the atypical box design studied.

Displacement at Compression Strength

Hansson [19] found out that the deformation of corrugated panels at failure when loaded in in-plane direction depends only on the geometry and the boundary conditions of the panels. Deformation does not depend on moisture content of the plates, deformation rate, or the dead-load in the creep test. In the current work, the displacement does not depend on the moisture content of the boxes, as Figure 7 shows. In the range of 2–11% moisture content, the displacement is constant, approximately 10mm. The result indicates that Hansson's observation can be extended to PE coated boxes with complex design. Failure criterion

for a specific box type in compression can be based on vertical displacement, and that it is independent of moisture content.

Deformation of Boxes

The stack of three boxes was compressed only 0.7 mm after the immediate fast compression due to placing the dead-load on top. Kirkpatrick [26] studied creep of polyethylene coated corrugated fiberboard boxes, and also noticed the low creep rate of the boxes. The displacement during secondary creep of one box was 1 mm when the box was exposed to cyclic 60/90% RH and 20°C for 8 days [26].

Figure 8 shows the box compression test curves of the creep tested boxes. BCT curves for boxes without the dead-loading, but with the same climate treatment are shown as reference. The exposure to dead-load has flattened the curve in the range of 1–5 mm, which is probably due to the crushing of crease lines. The effects of creep testing are to reduce the displacement at compression strength by approximately two millimeters.

Cyclic compression tests were done to interpret the BCT curves of the creep tested boxes, and to study the vertical deformation due to

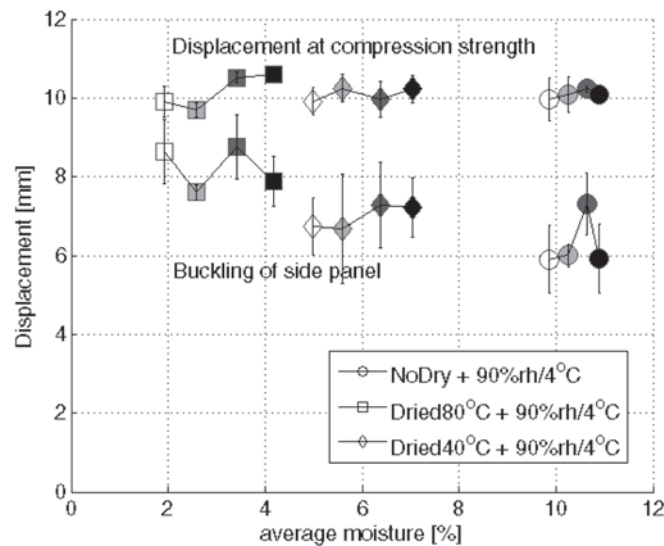


Figure 7. Vertical displacement at compression strength. Marker types: 'O' = non-pre-treated boxes (Case A), '◇' = pre-dried in 40°C (Case B), '□' = pre-dried in 80°C (Case C), Marker colors: white = references, gray = day 1, dark gray = day 4, black = day 8. Average and standard deviation (n = 3). Also the horizontal buckling of the side panel middle point at compression strength is shown.

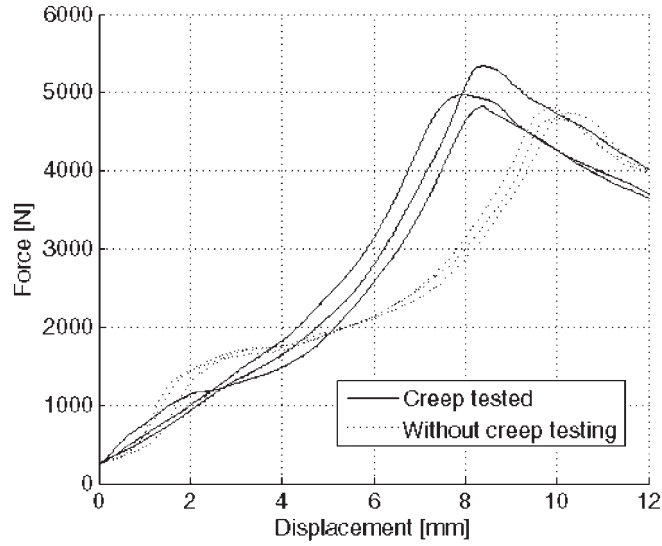


Figure 8. BCT curves of creep tested boxes (—), and boxes that were not creep tested (.....) after humidity treatment.

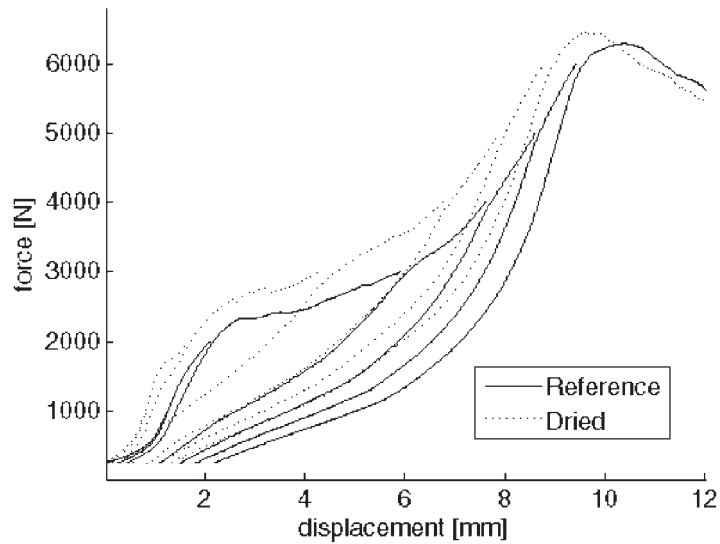


Figure 9. The cyclic BCT curves for a reference boxes (Ref) (—) and a pre-dried box (RefB) (.....).

repetitive loading more closely. The typical cyclic BCT curves (Figure 9) show that loads greater than 3000N–4000N follow a straighter curve than lower loads. Drying of the box does not change the shape of the BCT curves. When the boxes are loaded to over 2000N, the material starts gradually to yield and BCT curves similar to creep tested boxes are obtained. By comparing the slopes of cyclic BCT curves, it can be anticipated that the creaselines are not completely crushed during the creep test.

A box deforms permanently due to yielding of the material in each loading cycle. The duration of one loading-unloading cycle was between 30 s and 120 s. Permanent deformation was plotted as a function of total deformation for each loading cycle (Figures 10 and 11). Drying the boxes reduces the permanent deformation. The subsequent moistening increases the deformation, more so in the case where the boxes were dried before the exposure to humidity. Three boxes were also tested with 15 minutes hold time between each cycle. The permanent effect did not dependent on the hold time between the loading cycles.

The BCT curves of creep tested boxes are clearly different from the non-creep tested boxes. Curves were straighter, and the deformation at fracture was reduced by 2 mm. The compression strength was unaffected. The reduction of the deformation can be interpreted with the

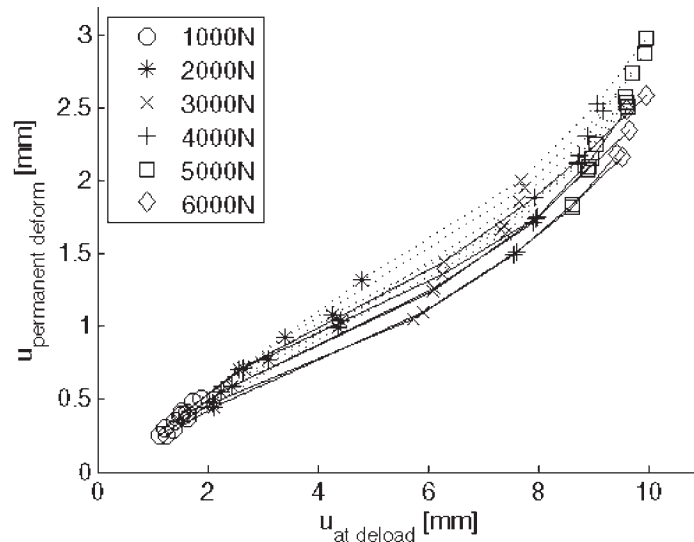


Figure 10. Permanent deformation of a box as a function of total deformation at unloading. (—) reference boxes (Ref), (.....) humidity treated boxes (Case A).

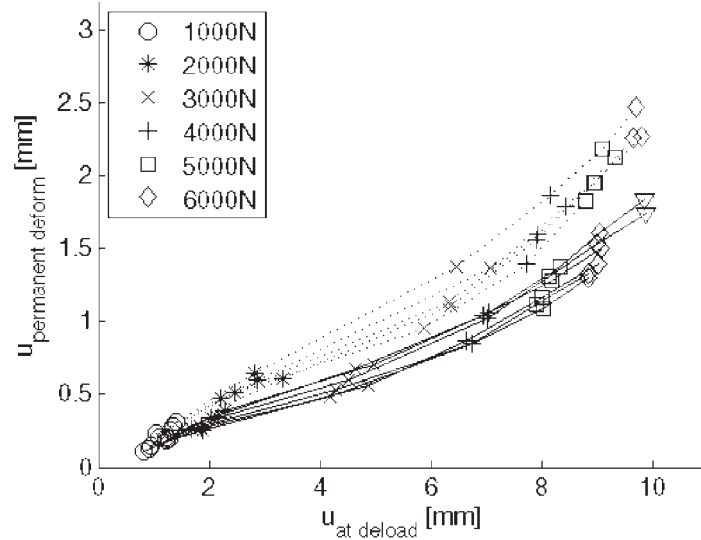


Figure 11. Permanent deformation of a box as a function of total deformation at unloading. (—) reference boxes (RefB), (.....) humidity treated boxes (Case B).

cyclic loading data. At the load level 2440 N, the permanent deformation is approximately 1.5 mm (see the curves after humidity treatment in Figure 10). The reduction of displacement in the creep test (2 mm) can be explained by the effect of creep (0.23 mm) and permanent deformation (1.5 mm). In the end-use situation, the load on the lowest box in a stack is approximately the same as in the creep test. During the usage of transport boxes, most of the displacement in box compression is due to plastic deformation of the creases. Thus at the conditions 90% RH, 4°C, and 40% of BCT load, the creep deformation accounts for less than 3% of the total deformation at failure. The 15 min hold time between the cycles of the cyclic testing produced similar results to the immediate loading results, which further confirms that the boxes do not show strong viscoelastic responses.

Buckling of the Long Box Panel

Figure 12 shows the typical shape of the box compression curve and the outward buckling of the mid-point point of the outer long side panel. The BCT curve starts quite flat due to the imperfections of the boxes. After a displacement around 0.5 mm, the slope increases, probably due to the initiation of compression and rotation of the upper and lower

crease lines. At 3–4 mm displacement, the force stops increasing, and the side panel starts buckling. At this point, the yielding of the creases is finished, and the stiffer panels strain. The slope of the buckling-displacement curve increases when the compression strength has been reached. At that point, visible kneeling lines 70–80 mm long appeared in the corners of the long panels, as has been reported earlier [8,13,14].

The buckling of the panel mid-point as a function of average moisture is shown in Figure 7. The data shows a slight decreasing trend, although there is a large variation in the results. The horizontal buckling of side panel decreases with increasing moisture content ($R^2 = -0.75$ for mean of buckling readings, $R^2 = -0.58$ for three parallel buckling readings). The vertical movement of the panel mid-point due to the outward buckling during the BCT testing is not accounted for in the data. In the BCT tests, the panels started to buckle after the first plateau had been reached. This also indicates that the first part of the loading causes the creases to yield. The buckling increased rapidly after the maximum force had been reached. The buckling of panels at the compression strength was found to decrease as the boxes got wetter. The results show that the fraction of plasticity deformation increases as the material moisture increases. Thus wetter the box wall is, the more it will deform vertically before it begins buckling.

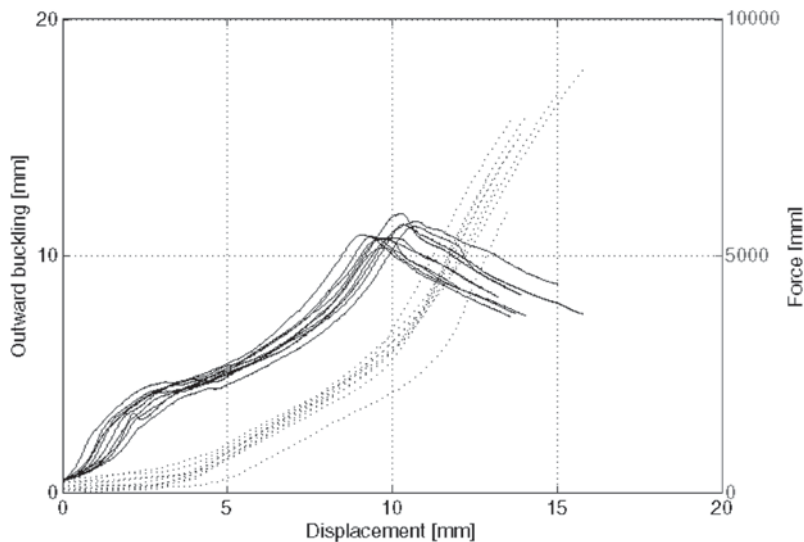


Figure 12. BCT curve (—) and outward buckling (.....) of the middle point of outer long side panel.

CONCLUSION

The results show that average moisture content is not well suited to describe moisture distribution of polyethylene coated boxes. PE restricts the moisture transport and leads to higher or lower moisture contents close to the open material edges. The compression strength was observed to decrease linearly at the rate of 380 N per one percent change in moisture content. During eight days of exposure to a high humidity environment (90% RH; 4°C), the boxes lost 15% of their compression strength and moisture content increased by 1%. The decrease of the BCT value in relation to the change in moisture content is comparable to earlier results for uncoated boxes. It takes longer for moisture content to change with PE coatings. Failure of the boxes in this study, can be expressed as a critical vertical displacement independent of moisture content. The viscoelastic effects were found to be small compared to the permanent deformation during the top-to-bottom loading. The magnitude of the permanent deformation increases with increasing moisture content. As a result, buckling decreased as moisture content increased.

ACKNOWLEDGEMENTS

The tests were done at Innventia in Stockholm, Sweden. The help of Lic. Eng. Thomas Trost on practical test arrangements and the discussions with Dr. Johan Alftan were valuable and are greatly appreciated. The materials for the test were provided by Peterson Emballege, Trondheim, Norway. Ms Gunvor Levang is appreciated for the box shipments to Stockholm. The Research Council of Norway, Peterson AS, Eka Chemicals AB, and the Foundation of Paper and Fiber Reserch Institute in Trondheim, Norway (PFI) are gratefully acknowledged for the financial support.

REFERENCES

1. Salmen, L., Responses of paper properties to changes in moisture content and temperature, in Tenth fundamental research symposium at Oxford, Vol.1. 1993, Pira International: Surrey, UK. p. 369–430.
2. Kellicutt, K.Q. and E.F. Landt, Development of design data for corrugated fiberboard shipping containers. *Tappi*, 1952. 35(9): p. 398–402.
3. Kellicutt, K.Q., Compressive strength of boxes. *Package Engineering*, 1960. 5(2): p. 94–96.
4. Carlson, D.A., Box compression variation. *Corrugating Int*, 2002. 4(2): p. 7–9.
5. Kellicutt, K.Q., Effect of contents and load bearing surface on compressive strength and stacking life of corrugated containers. *Tappi*, 1963. 46(1): p. 151A–154A.

6. Kellicutt, K.Q., Compressive strength of boxes—Part I. *Package Engineering*, 1959. 4(12): p. 88–89.
7. Peterson, W.S. and T.S. Fox, Workable Theory Proves How Boxes Fail in Compression. *Paperboard Packaging*, 1980. 65(10): p. 136–140, 142–144.
8. Maltenfort, G.G., Compression load distribution on corrugated boxes. *Paperboard Packaging*, 1980. 65(9): p. 71–72, 74, 76–78, 80.
9. Meng, G., T. Trost, and S. Östlund, Stacking misalignment of corrugated boxes—a preliminary study, in 23rd IAPRI Symposium on Packaging, 3–5 September 2007. 2007: Windsor UK. p. 19.
10. Peterson, W.S. and W.J. Schimmelpfenning, Panel edge boundary conditions and compressive strengths of tubes and boxes. *Tappi*, 1982. 65(8): p. 108–110.
11. Beldie, L., G. Sandberg, and L. Sandberg, Paperboard packages exposed to static loads—finite element modelling and experiments. *Packaging Technology and Science*, 2001. 14(4): p. 171–178.
12. Packaging—Complete, filled transport packages—Compression and stacking tests using a compression tester. ISO 12048-2:1994.
13. McKee, R.C. and J.W. Gander, Top-Load Compression. *Tappi*, 1957. 40(1): p. 57–64.
14. Srihiran, J., L. Jarupan, and T. Jinkarn, The Analysis of Dimensional Changes Impacts on Compression Strength of Corrugated Box by Finite Element Method, in 16th IAPRI World Conference on Packaging, June 8–12, 2008. 2008: Bangkok, Thailand.
15. Popil, R.E., D.W. Coffin, and C.C. Habeger, Transverse shear measurement for corrugated board and its significance. *Appita Journal*, 2008. 61(4): p. 307–312.
16. Rahman, A.A. Finite element buckling analysis of corrugated fiberboard panels. 1997. Evanston, IL, USA: ASME.
17. Marcondes, J.A., Effect of load history on the performance of corrugated fibreboard boxes. *Packaging technology and science*, 1992. 5(4).
18. Kellicutt, K.Q., Structural notes for corrugated containers. Note no 13: Compressive strength of boxes—Part III. *Package Engineering*, 1960. 5(2): p. 94–96.
19. Hansson, T., Deformation based failure criterion for corrugated board panels, in *Solid Mechanics*. 2008, KTH: Stockholm. p. 31.
20. Harte, B.R., et al., Compression strength of corrugated shipping containers held in frozen storage. *Boxboard Containers*, 1985. 93(2): p. 17–23.
21. Lyngå, H. and G. Sikö, Moisture dynamics in corrugated board boxes, in *Structural mechanics*. 2003, Lund University: Lund. p. 72.
22. Morgan, D.G. A Mechanistic Creep Model and Test Procedure. 2003. Melbourne, Vic., Australia: Appita Inc.
23. Leake, C.H. and R. Wojcik, Humidity cycling rates: how they influence container life spans. *Tappi*, 1993. 76(10): p. 26–30.
24. Fellers, C. and J. Panek, Effect of relative humidity cycle start point and amplitude on the mechano-sorptive creep of containerboard, in 61st Appita annual conference and exhibition. 2007: Gold Coast, Australia, 6–9 May 2007.
25. Coffin, D.W., The creep response of paper: review, in *Advances in Paper Science and Technology: 13th fundamental research symposium*, Cambridge, 11–16 Sept. 2005, [Pulp and Paper Fundamental Research Society, 2005, 3 vols (ISBN 0954527232)], S.J. I'Anson, Editor. 2005. p. vol 2. 651–747.
26. Kirkpatrick, J. and G. Ganzenmuller, Engineering Corrugated Packages to Survive Cyclic Humidity Environments—A Case Study, in 3d International Symposium, Moisture and Creep Effects on Paper, Board and Containers, I.R. Chalmers, Editor. 1997: Rotorua, New Zealand, 20–21 February 1997. p. 257–264.
27. Bronkhorst, C.A., Towards a more mechanistic understanding of corrugated container creep deformation behaviour. *Journal of Pulp and Paper Science*, 1997. 23(4): p. J174–J181.
28. Considine, J.M. and T.L. Laufenberg, Literature Review of Cyclic Humidity Effects on Paper-

- board Packaging, in *Cyclic Humidity Effects on Paperboard Packaging*, T.L. Laufenberg and C.H. Leake, Editors. 1992, TAPPI, USDA: Madison, Wisconsin, USA. p. 1–10.
29. Singh, S.P., Stability of Stacked Pallet Loads and Loss of Strength in Stacked Boxes Due to Misalignment, in *4th International symposium—Moisture and Creep Effects on Paper, Board and Containers*, J.-M. Serra-Tosio and I. Vullierme, Editors. 1999, E.F.P.G.: Grenoble, France, 18–19 March, 1999. p. 16–25.

Dynamics of Product-Transport-System by Improved Inverse Sub-structuring Method

WANG JUN^{1,2,*}, LU LI-XIN^{1,2} and WANG ZHI-WEI³

¹Department of Packaging Engineering, Jiangnan University, Wuxi 214122 PRC

²Key laboratory of food packaging techniques & safety of
China national packaging corporation, Wuxi 214122 PRC

³Packaging Engineering Institute, Jinan University, Zhuhai 519070, PRC

ABSTRACT: Product, packaging and vehicle constitute a complex product-transport-system in logistics. It's very difficult to model the complex interaction between the packaged product and vehicle. In this paper, the system is partitioned into three components as critical component (the damage of most products usually occurs firstly at the so-called critical component), product and vehicle. In the new model, the product and vehicle are connected through internal and external packaging, container, pallet, and other auxiliary devices (nail, rope, bundled device, etc.), and Then a new spectral-based formulation for predicting the dynamic characteristics of the complex interaction for product-transport-system is developed. By using a lumped-parameter representation, the proposed method is theoretically verified, and the critical parameters affecting the dynamic response of the coupled system are identified. The effects of the coupling stiffness, frequency parameter ratio and damping on the dynamic response of critical component are investigated. Reducing the coupling stiffness of product-vehicle interface may lead to lower response of critical component. There is a sensitive range around 1 of frequency parameter ratio, where the response of critical component is largely amplified. It should be noted that one can effectively lower the response of critical component by increasing the damping between critical component and main body of product when the frequency parameter ratio is less than 1, and/or by increasing the damping of the product-vehicle coupling interface when the frequency parameter ratio is larger than 1. The results may lead to some insights into the dynamic characteristics of the product-transport-system.

1.0 INTRODUCTION

IN the past, great efforts have been made in the field of packaging dynamics analysis and product damage evaluation. Newton's damage

*Author to whom correspondence should be addressed. E-mail: wangj_1982@jiangnan.edu.cn

boundary concept [1] and succeeding modified damage evaluation approaches, such as fatigue damage boundary concept [2], displacement damage boundary concept [3], dropping damage boundary concept [4], bruising boundary concept [5], damage boundary surface concept [6], were widely utilized in packaging design. Despite the popularity of these concepts, some basic assumptions of all these theories have been questioned: (1) the packaged product was isolated from the vehicle; (2) the packaging interface between the product and the vehicle was treated as simple linear or nonlinear spring. These may not be valid.

In logistics, product, packaging and vehicle constitute a complex product-transport-system [7]. It's very difficult to obtain the dynamic response of the product-transport-system under the excitation of environmental vibration and shock because of the complex interaction between the packaged product and vehicle. A considerable amount of experimental work and a few simulation models associated with some simple laboratory tests have been done by others to investigate the dynamics of the complex system [8–12]. Packaging designers are finding that these trial-and-error approaches presently used to control undesirable vibration response are not only time consuming and costly, but also do not lead to the optimal solution.

The competitiveness of the global logistics market and demand from product protection have made it necessary to develop more accurate analysis and modeling techniques to investigate the dynamical characteristics of the product-transport-system. In general, a product-transport-system is composed of many individual components such as the critical component, the product, the vehicle, etc. Vibration of the critical component due to the interaction between the tire and the road is typically of concern in packaging design. The biggest challenge remaining is the modeling of the coupling packaging interface [11].

However, the packaging interface is very complex and difficult to model. Traditional parameter identification methods [13] may be not suitable for the complex coupling packaging interface. Lim et al. [14–15] developed a spectral-based inverse substructuring method to predict the response functions of discretely connected structures from response spectra of the coupled system. Then, it was applied to investigate the vibration transmissibility and frequency response characteristics of motor vehicle structures, and reveal the application prospect of the method to a complex structure, such as the product-transport-system [16–17]. However, because of the complexity of the coupling packaging interface, the original version of inverse substruct-

turing method for two-substructure coupled system is not suitable for product-transport-system.

In this paper, product-transport-system is considered as a three-substructure coupled system composed of critical component, product and vehicle connected by complex packaging interface. Based on the inverse substructure method, a three-level indirect inverse substructuring method was developed and applied to predict the coupling stiffness of packaging interface. The validation of the proposed method is conducted by numerical calculation. The effects of the product parameters and packaging interface on the dynamic response of critical component are also investigated.

2. MODELLING AND EQUATIONS

The product-transport-system can be simplified to be represented by a discretized model as shown in Figure 1 [18]. The rigid mass m_2 is assumed to represent the mass of the product, to which the mass of critical component m_1 is attached by a linear spring of stiffness k_1 and linear viscous damper c_1 ; k_2 and c_2 denote respectively the equivalent coupling stiffness and damping of the packaging interface between the packaged product and vehicle. The system C representing the vehicle is modeled by a one-track semi-vehicle model, where, m_3 , m_4 and m_5 denote respectively the mass of half-bodywork, trailing-wheel and front-

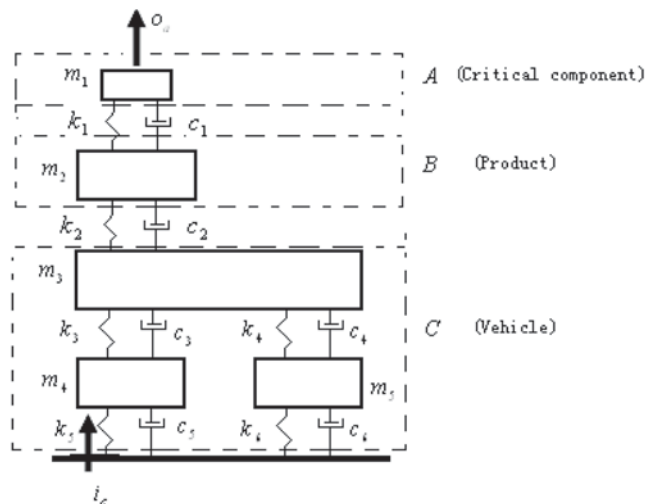


Figure 1. The lumped-parameter model of product-transport-system.

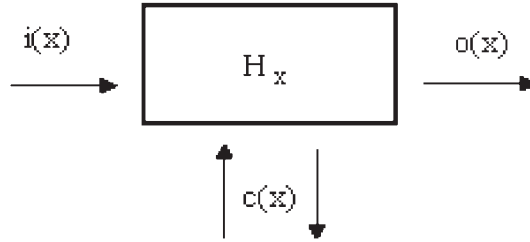


Figure 2. A general substructure representation.

wheel. And k_i, c_i denote respectively the stiffness and damping of the vehicle ($i = 3, 4, 5, 6$ denote respectively that of the trailing and front suspension and that of the trailing and front tire).

A complex system can always be decomposed into a number of sub-structural systems. Given a substructure shown in Figure 2, which can be generally represented by a set of frequency response functions (FRF) $[H_x]$ relating two sets of reference and response coordinates, the relationship can be expressed as

$$\begin{Bmatrix} X_{o(x)} \\ X_{c(x)} \end{Bmatrix} = \begin{bmatrix} H_{x,o(x)i(x)} & H_{x,o(x)c(x)} \\ H_{x,c(x)i(x)} & H_{x,c(x)c(x)} \end{bmatrix} \begin{Bmatrix} F_{i(x)} \\ F_{c(x)} \end{Bmatrix} \quad (1)$$

For a product-transport-system, it can be partitioned into three components as substructure *A* (critical component), substructure *B* (product), and substructure *C* (vehicle), as shown in Figure 3.

To obtain the system-level transfer functions, substructure *A* and substructure *B* was firstly coupled as *D*. Applying the linear system theory to each individual substructure and enforcing the displacement compatibility and force equilibrium conditions, we get

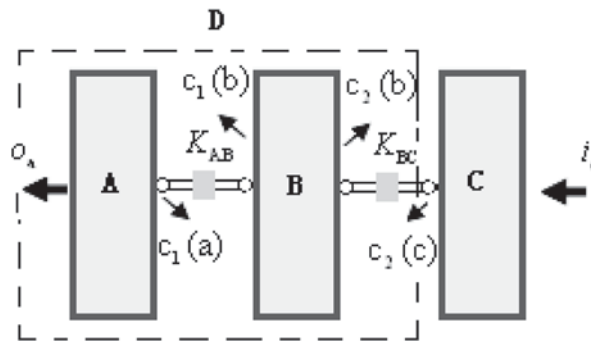


Figure 3. A three-component coupled product-transport-system.

$$\begin{aligned}
& \begin{bmatrix} H_{D,o(a)i(a)} & H_{D,o(a)c_1(x)} & H_{D,o(a)i(b)} \\ H_{D,c_1(x)i(a)} & H_{D,c_1(x)c_1(x)} & H_{D,c_1(x)i(b)} \\ H_{D,o(b)i(a)} & H_{D,o(b)c_1(x)} & H_{D,o(b)i(b)} \end{bmatrix} = \\
& \begin{bmatrix} H_{A,o(a)i(a)} & H_{A,o(a)c_1(x)} & 0 \\ H_{X,c_1(x)i(a)} & H_{X,c_1(x)c_1(x)} & H_{X,c_1(x)i(b)} \\ 0 & H_{B,o(b)c_1(x)} & H_{B,o(b)i(b)} \end{bmatrix} - \quad (2) \\
& \begin{bmatrix} \alpha H_{A,o(a)c_1(a)} \\ H_{X,c_1(x)c_1(x)} \\ \beta H_{B,o(b)c_1(b)} \end{bmatrix} [D_{AB}] [\alpha H_{A,c_1(a)i(a)} \quad H_{X,c_1(x)c_1(x)} \quad \beta H_{B,c_1(b)i(b)}]
\end{aligned}$$

where,

$$D_{AB} = (H_{A,c_1(a)c_1(a)} + H_{B,c_1(b)c_1(b)} + K_{AB}^{-1})^{-1}, \quad \alpha = \begin{cases} 1 & x = a, X = A \\ -1 & x = b, X = B \end{cases}$$

$$\beta = \begin{cases} 1 & x = b, X = B \\ -1 & x = a, X = A \end{cases}$$

By cascading the similar coupling process for substructure *C* and substructure *D*, we get

$$\begin{aligned}
& \begin{bmatrix} H_{S,o(d)i(d)} & H_{S,o(d)c_2(x)} & H_{S,o(d)i(c)} \\ H_{S,c_2(x)i(d)} & H_{S,c_2(x)c_2(x)} & H_{S,c_2(x)i(c)} \\ H_{S,o(c)i(d)} & H_{S,o(c)c_2(x)} & H_{S,o(c)i(c)} \end{bmatrix} = \\
& \begin{bmatrix} H_{D,o(d)i(d)} & H_{D,o(d)c_2(x)} & 0 \\ H_{X,c_2(x)i(d)} & H_{X,c_2(x)c_2(x)} & H_{X,c_2(x)i(c)} \\ 0 & H_{C,o(c)c_2(x)} & H_{C,o(c)i(c)} \end{bmatrix} - \quad (3) \\
& \begin{bmatrix} \alpha H_{A,o(a)c_1(a)} \\ H_{X,c_1(x)c_1(x)} \\ \beta H_{B,o(b)c_1(b)} \end{bmatrix} [D_{AB}] [\alpha H_{A,c_1(a)i(a)} \quad H_{X,c_1(x)c_1(x)} \quad \beta H_{B,c_1(b)i(b)}]
\end{aligned}$$

where,

$$D_{DC} = (H_{D,c_2(d)c_2(d)} + H_{C,c_2(c)c_2(c)} + K_{BC}^{-1})^{-1}, \quad \alpha_1 = \begin{cases} 1 & x = d, X = D \\ -1 & x = c, X = C \end{cases},$$

$$\beta_1 = \begin{cases} 1 & x = c, X = C \\ -1 & x = d, X = D \end{cases}$$

Equations (2) and (3) can be combined into a matrix form spectral-based substructuring formulation that expresses the system's frequency response in terms of the transfer functions of the free substructures. For product-transport-system, we are most concerned about the system-level response of critical component due to the excitation of i_c (tire-road interaction). Here we give the expression of system's frequency response $H_{S,o(a)i(a)}$

$$\begin{aligned} H_{S,o(a)i(c)} &= H_{A,o(a)c_1(a)} [H_{A,c_1(a)c_1(a)} + H_{B,c_1(b)c_1(b)} + K_{AB}^{-1}]^{-1} H_{B,c_1(b)c_2(b)} \\ &\{H_{B,c_2(b)c_2(b)} - H_{B,c_2(b)c_1(b)} [H_{A,c_1(a)c_1(a)} + H_{B,c_1(b)c_1(b)} + K_{AB}^{-1}]^{-1} H_{B,c_1(b)c_2(b)} \\ &+ H_{C,c_2(c)c_2(c)} + K_{BC}^{-1}\}^{-1} H_{C,c_2(c)i(c)} \end{aligned} \quad (4)$$

When all FRFs and coupling stiffness in the right side of Equation (4) can be measured or computed, $H_{S,o(a)i(a)}$ can be predicted. For product-transport-system, it's almost impossible to measure directly the coupling stiffness of packaging interface between product and vehicle because of the complex interaction (including internal and external packaging, container, pallet, nail, rope, bundled device, etc.).

In order to obtain the coupling stiffness of packaging interface, the inverse substructuring method proposed by Lim is applied [14], and the coupling stiffness of the packaging interface can be predicted by following formulation

$$K_{BC} = \frac{H_{S,c_2(b)c_2(b)}}{H_{S,c_2(b)c_2(b)} H_{S,c_2(c)c_2(c)} - H_{S,c_2(b)c_2(c)}^2} \quad (5)$$

Similarly, the coupling stiffness of interface between critical component and product can be obtained as

$$K_{AB} = \frac{H_{S,c_1(a)c_1(b)}}{H_{S,c_1(a)c_1(a)} H_{S,c_1(b)c_1(b)} - H_{S,c_1(a)c_1(b)}^2} \quad (6)$$

Equation (5) gives us a method to predict the coupling stiffness of packaging interface by measured system-level FRFs. However, the coupling packaging interface is usually surface connection, and it's difficult to monitor the vibration response or execute hammer excitation at the packaging interface, all FRFs in the right side of Equation (5) can not easily be measured for a coupled product-transport-system.

To solve this problem, the coupling stiffness of packaging interface is solved from Equation (4) as

$$K_{BC} = \{H_{C,c_2(c)i(c)}H_{S,o(a)i(c)}^{-1}H_{A,o(a)c_1(a)}[H_{A,c_1(b)c_1(b)} + K_{AB}^{-1}]^{-1}H_{B,c_1(b)c_2(b)} - H_{B,c_2(b)c_2(b)} + H_{B,c_2(b)c_1(b)}[H_{A,c_1(a)c_1(a)} + H_{B,c_1(b)c_1(b)} + K_{AB}^{-1}]^{-1}H_{B,c_1(b)c_2(b)} - H_{C,c_2(c)c_2(c)}\}^{-1} \quad (7)$$

Substituting Equation (6) into Equation (7), we get

$$K_{BC} = \{H_{C,c_2(c)i(c)}H_{S,o(a)i(c)}^{-1}H_{A,o(a)c_1(a)}[H_{A,c_1(a)c_1(a)} + H_{B,c_1(b)c_1(b)} + (H_{S,c_1(a)c_1(a)}H_{S,c_1(b)c_1(b)} - H_{S,c_1(a)c_1(b)}^{-1})^{-1}H_{B,c_1(b)c_2(b)} - H_{B,c_2(b)c_2(b)} + H_{B,c_2(b)c_1(b)}[H_{A,c_1(a)c_1(a)} + H_{B,c_1(b)c_1(b)} + (H_{S,c_1(a)c_1(a)}H_{S,c_1(b)c_1(b)} - H_{S,c_1(a)c_1(b)}^{-1})^{-1}H_{B,c_1(b)c_2(b)} - H_{C,c_2(c)c_2(c)}\}^{-1} \quad (8)$$

For product-transport-system, the measurement of component-level FRFs of critical component, product, as well as vehicle is often readily available, and the coupling interface between the critical component and product is convenient for vibration response monitoring and hammer excitation. Equation (8) gives us another feasible method for predicting coupling stiffness of packaging interface by a series of measured FRFs. This approach avoided the difficult issues of vibration response monitoring or hammer excitation at the packaging interface.

3. RESULTS AND DISCUSSIONS

3.1 Numerical Validation

In order to validate the theory proposed, a numerical study is applied to the lumped-parameter model of product-transport-system shown in Figure 1. The system is partitioned into three components as substructure *A* (critical component), substructure *B* (product), and substructure *C* (vehicle). Their specific parameters are given in Table 1 [18].

Table 1. Parameters of the Lumped Product-Transport-System.

Mass (kg)	Stiffness (N/m)	Damping (Ns/m)
$m_1 = 0.5$	$k_1 = 2000$	$c_1 = 1$
$m_2 = 5$	$k_2 = 6000$	$c_2 = 10$
$m_3 = 600$	$k_3 = 22000$	$c_3 = 1500$
$m_4 = 45.5$	$k_4 = 17000$	$c_4 = 1500$
$m_5 = 40.5$	$k_5 = 192000$	$c_5 = 0$
	$k_6 = 192000$	$c_6 = 0$

The general equations of motion governing the dynamic response of the three free sub-structures in the disconnected state and the coupled system are

$$[M_w]\{\ddot{X}_w\} + [C_w]\{\dot{X}_w\} + [K_w]\{X_w\} = \{F_w\} \quad w = A, B, C, S \quad (9)$$

where $[M]$, $[C]$ and $[K]$ are the assembled mass, damping and stiffness matrices respectively of the model in question, i.e., $w = A, B, C$ or S referring to sub-structure A, B, C or system S . These matrices are expressed explicitly as

(1) Sub-structure A

$$[M_A] = [m_1] \quad (10)$$

$$[K_A] = [0] \quad (11)$$

$$[C_A] = [0] \quad (12)$$

(2) Sub-structure B

$$[M_B] = [m_2] \quad (13)$$

$$[K_B] = [0] \quad (14)$$

$$[C_B] = [0] \quad (15)$$

(3) Sub-structure C

$$[M_C] = \begin{bmatrix} m_3 & 0 & 0 \\ 0 & m_4 & 0 \\ 0 & 0 & m_5 \end{bmatrix} \quad (16)$$

$$[K_C] = \begin{bmatrix} k_3 + k_4 & -k_3 & -k_4 \\ -k_3 & k_3 + k_5 & 0 \\ -k_4 & 0 & k_4 + k_6 \end{bmatrix} \quad (17)$$

$$[C_c] = \begin{bmatrix} c_3 + c_4 & -c_3 & -c_4 \\ -c_3 & c_3 + c_5 & 0 \\ -c_4 & 0 & c_4 + c_6 \end{bmatrix} \quad (18)$$

(4) System S

$$[M_S] = \begin{bmatrix} m_1 & 0 & 0 & 0 & 0 \\ 0 & m_2 & 0 & 0 & 0 \\ 0 & 0 & m_3 & 0 & 0 \\ 0 & 0 & 0 & m_4 & 0 \\ 0 & 0 & 0 & 0 & m_5 \end{bmatrix} \quad (19)$$

$$[K_S] = \begin{bmatrix} k_1 & -k_1 & 0 & 0 & 0 \\ -k_1 & k_1 + k_2 & -k_2 & 0 & 0 \\ 0 & -k_2 & k_2 + k_3 + k_4 & -k_3 & -k_4 \\ 0 & 0 & -k_3 & k_3 + k_5 & 0 \\ 0 & 0 & -k_4 & 0 & k_4 + k_6 \end{bmatrix} \quad (20)$$

$$[C_S] = \begin{bmatrix} c_1 & -c_1 & 0 & 0 & 0 \\ -c_1 & c_1 + c_2 & -c_2 & 0 & 0 \\ 0 & -c_2 & c_2 + c_3 + c_4 & -c_3 & -c_4 \\ 0 & 0 & -c_3 & c_3 + c_5 & 0 \\ 0 & 0 & -c_4 & 0 & c_4 + c_6 \end{bmatrix} \quad (21)$$

Assuming forced periodic excitation, the steady-state vibratory response in frequency domain is

$$\{X_m\} = (-\omega^2[M_w] + j\omega[C_w] + [K_w]^{-1}\{F_w\}) = [H_w]\{F_w\} \quad (22)$$

where ω is the excitation frequency. This form is used to generate the necessary FRFs of the free sub-structures and coupled system.

All FRFs needed in the right side of Equation (8) are computed to predict the coupling stiffness of packaging interface, and the predicted dynamic stiffness applying Equation (8) is compared with the exact coupling terms. The result is shown in Figure 4, from the plot, we find that the predicted dynamic stiffness is in exact agreement with the "Given" (the value in Table 1).

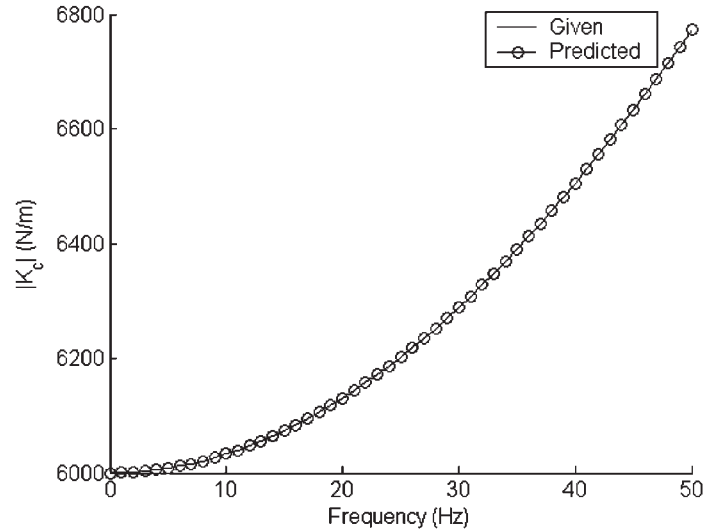


Figure 4. Comparison of the predicted and exact coupling stiffness of packaging interface.

3.2 Response of Critical Component

3.2.1 Effect of Coupling Stiffness

Equation (8) offers us a new approach to predict the coupling stiffness of packaging interface. Substituting Equation (8) into Equation (4), the system response of product-transport-system can be predicted. As the coupling packaging interface represents the only vibratory energy transmission path between the packaged product and vehicle, it's of interest to gain a better understanding of their effects on system response. In general, the overall system response tends to reduce with the decrease of coupling packaging stiffness if other parameters are unchanged. This trend can be clearly seen in Figure 5.

3.2.2 Effect of Frequency Parameter Ratio

As studied for isolated packaged product system by Schell and Jiang [19,20], the effect of frequency parameter ratio of critical component to product on the response of critical component is noticeable. Now we discuss the case of product-transport-system when considering the complex interaction between the packaged product and vehicle. Defining $\omega_1 = \sqrt{k_1/m_1}$ and $\omega_2 = \sqrt{k_2/m_2}$ respectively as frequency

parameter of critical component and product, we get the frequency parameter ratio as $\lambda_1 = \omega_1/\omega_2$.

A new parameter was introduced to address the effect of frequency parameter ratio on the dynamic response of critical component as:

$$\Gamma = \sqrt{\sum_{f=0}^{50} |H_{S,o(a)i(b)}|^2 \Delta f}$$

Γ represents the sum of mean-square of a function in a specific frequency range.

Figure 6 shows the effect of frequency parameter ratio on the response of the critical component, indicating that the response of the critical component increases first and decreases afterwards when increasing the frequency parameter ratio. There is a sensitive range around 1 of frequency parameter ratio, where the response of critical component is largely amplified. It should be avoided when design packaging interface. Moreover, it's shown that the response of critical component can be effectively decreased by increasing the damping between critical component and product when the frequency parameter ratio is less than 1, and/or increasing the damping of product-vehicle coupling interface when the frequency parameter ratio is larger than 1.

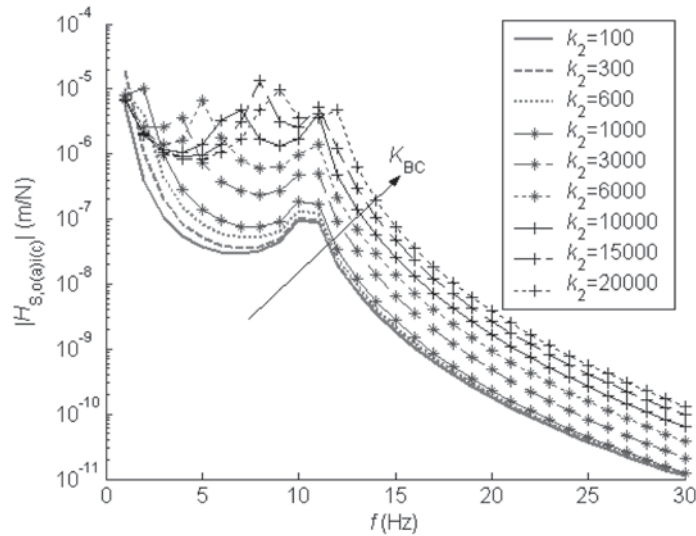


Figure 5. Effect of coupling packaging stiffness on assembled system FRF represented by $H_{S,o(a)(a)}$.

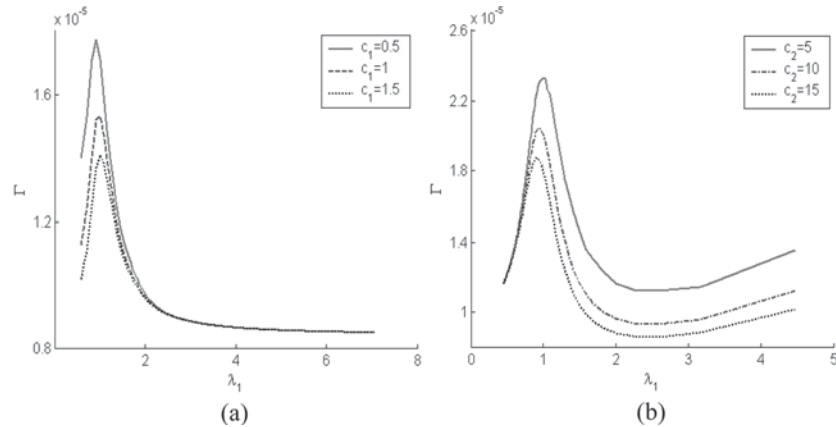


Figure 6. Effect of frequency parameter ratio on system response: (a) with varying damping of critical component-product coupling interface; (b) with varying damping of product-vehicle coupling interface.

4. CONCLUSION

In this paper, a spectral-based formulation is derived based on inverse substructuring method. The proposed theory offers an approach to back out the coupling stiffness between packaged product and vehicle for product-transport-system. Application of this approach to an idealized lumped product-transport-system leads to following finding that are also applicable to other comparable structures:

1. Reducing the coupling stiffness of packaging interface leads to lower system response of critical component.
2. There is a sensitive range around 1 of frequency parameter ratio, where the response of critical component is largely amplified. It should be avoided when design packaging interface.
3. It should be noted that one can effectively lower the response of critical component by increasing the damping between critical component and main body of product when the frequency parameter ratio is less than 1, and/or by increasing the damping of the product-vehicle coupling interface when the frequency parameter ratio is larger than 1.

ACKNOWLEDGEMENTS

The authors would like to gratefully acknowledge this support by

Project of Innovative Research Team of Jiangnan University (PIRTJiangnan), Natural Science Foundation of Jiangnan Universities and Fundamental Research Funds for the Central Universities (JUSRP11009).

REFERENCES

1. Newton, R.E., "Fragility assessment theory and practice", Monterey Research Laboratory, Inc. Monterey, California, 1968.
2. Burgess, G.J., "Product Fragility and Damage Boundary Theory", *Packaging Technology and Science*, Vol.15, 1988, pp.5–10.
3. Wang, Z.L., Wu, C.F. and Xi, D.C., "Damage boundary of a packaging system under rectangular pulse excitation", *Packaging Technology and Science*, Vol.11, 1998, pp.189–202.
4. Wang, Z.W., "On evaluation of product dropping damage", *Packaging Technology and Science*, Vol.15, 2002, pp.115–120.
5. Lu, L.X., Wang, Z.W., "Dropping bruise fragility and bruise boundary of apple fruit", *Transaction of ASABE*, Vol.50, 2007, pp.1323–1329.
6. Wang, J, Wang, Z.W., "Damage boundary surface of a tangent nonlinear packaging system with critical components", *Journal of vibration and shock*, Vol.27, 2008, pp.166–167, 185.
7. Wang, J., Wang, Z.W, Hu, C.Y., "Investigation on dynamical characteristics of product-transport-system", Proceedings of the 12th Chinese packaging conference, *Zhuhai*, 2008.
8. Urbanik, T. J., "Transportation vibration effects on unitized corrugated containers", United State Department of Agriculture, Forest Service Research Paper FPL, Vol. 22, 1978, pp.1–24.
9. School, D, Holt, J.E., "Road-vehicle-load interaction for transport of fruit and vegetables", *Agricultural systems*, Vol. 8, 1982, pp. 143–155.
10. Peleg, K, Hinga, S., "Simulation of vibration damage in produce transportation", *Transactions of the ASAE*, Vol. 29, 1986, pp. 633–641.
11. Xu, W.M., Sun, G.Z., "Numerical simulation of packaging product dynamic response under road pulse excitation", *Packaging Engineering*, Vol. 25, 2004, pp.163–165.
12. Jagjit Singh, S. Paul Singh, Eric Joneson, "Measurement and analysis of US truck vibration for leaf spring and air ride suspensions, and development of tests to simulate these conditions", *Packaging Technology and Science*, Vol. 19, 2006, pp. 309–323.
13. Yang, B.Y., Song, Y.G., "A substructure method of parameter identification for joining stiffness on interfaces", *Chinese Quarterly of Mechanics*, Vol. 22, 2001, pp. 420–427.
14. Zhen, J., Lim, T.C., Lv, G.Q., "Determination of system vibratory response characteristics applying a spectral-based inverse sub-structuring approach. Part I: analytical formulation", *Int. J. Vehicle Noise and Vibration*, Vol. 1, 2004, pp.1–30.
15. Zhen, J., Lim, T.C., Lv, G.Q., "Determination of system vibratory response characteristics applying a spectral-based inverse sub-structuring approach. Part II: motor vehicle structures", *Int. J. Vehicle Noise and Vibration*, Vol. 1, 2004, pp. 31–67.
16. Lv, G.Q., Wang, Z.W., Wang, L., "Inverse sub-structuring analysis and computations of dynamic characteristics of transportation packaging system", *Packaging Engineering*, Vol. 27, 2006, pp.49–51.
17. Wang, Z.W, Wang, J, Hu, C.Y., "Investigation into the dynamical characteristics of packaging system based on critical component by applying the inverse substructuring method", The 16th IAPRI Conference, Bangkok, 2008.
18. Crolla, D. 2004. Vehicle dynamics and control. China Communications Press, Beijing.
19. Schell, E.H., "Evaluation of a fragility test method and some proposals for simplified methods", *Shock Vibration Bull.*, Vol. 40, pp. 133–152.
20. Jiang J.H., Wang Z.W., "Study of the shock response of packaging system under half-Sine excitation", *Packaging Engineering*, Vol. 28, 2007, pp. 4–5.

Effect of Freeze-Thaw Cycling on the Compression Strength of Folding Cartons made from Different Materials

KOUSHIK SAHA^{1,*}, BRUCE HARTE², GARY BURGESS² and SUJEET ADUDODLA³

¹*Assistant Professor, Industrial Technology CalPoly State University, San Luis Obispo, CA 93407*

²*Professors, School of Packaging, Michigan State University, East Lansing, MI 48824*

³*Research Associate, School of Packaging, Michigan State University, East Lansing, MI 48824*

ABSTRACT: The quality of frozen food is known to deteriorate in storage due to water migration, in-pack desiccation and frost formation. These same factors can affect folding cartons. The rate of frozen food and folding carton deterioration is further dependent on temperature fluctuations during storage, transportation, loading and unloading. This study was conducted to compare the compression strength of folding cartons made from CNK (Coated Natural Kraft), SBS (Solid Bleached Sulfate), CRP (Coated recycled paperboard) and PCSBS (Poly coated Solid Bleach Sulfate) after subjecting them to multiple freeze-thaw cycles. Compression tests were performed on empty cartons and cartons filled with frozen peas. A two inch headspace was maintained above the peas to prevent them from contributing to carton compression strength. The moisture content of all four carton materials was also determined for all treatments. CNK cartons showed better capacity to withstand compression compared to folding cartons made from SBS, CRP and PCSBS, following freeze thaw cycling.

INTRODUCTION

A large portion of frozen foods are packaged in folding cartons. Approximately 75% of all folding cartons in a supermarket frozen food case are made of SBS (Solid Bleach Sulfate) and less than 10% are made of CNK (Coated Natural Kraft) as reported by a major carton material supplier [1]. There has been a long standing debate about the type of carton material needed to reduce unsaleables caused by carton

*Author to whom correspondence should be addressed. E-mail: ksaha@calpoly.edu

damage. Damaged cartons and containers led to 2.57 billion dollars in losses to the consumer packaging industry for the year 2004 [2]. An independent audit firm found that most of the frozen food carton damage occurred after reaching the supermarket loading dock [2]. Therefore, there is a critical need to develop a carton material that can withstand the rigors of a frozen food distribution system.

The quality of frozen food is known to deteriorate at freezing temperatures due to water migration, in-pack desiccation and frost formation. The rate of frozen food and folding carton deterioration is further dependent on temperature fluctuations in the storage chamber and abrupt increases in temperature during loading and unloading of product during distribution and transportation [2]. Freeze/thaw cycling leads to crystal growth and frost formation on food surfaces and the inner side of packages, such as folding cartons. Therefore surface coating on the exterior wall of the carton is not effective in stopping moisture uptake from the crystals formed inside the pack. Crystal growth and frost formation can be further explained by water migration from the product and in-pack desiccation.

When the temperature in the void volume of a package is lower than in the product, water vapor will transfer from the higher vapor pressure region (within product) to a region of lower vapor pressure, i.e. product surface or inner surface of a package. Moisture is not able to migrate back into the product but accumulates on its surface. This phenomenon is known as water migration. This enables smaller crystals to grow larger by adhering to free water molecules [3] thus accumulating on the product surface and internal surface of the folding carton. Such crystals grow at a faster rate with fluctuating temperatures [4,5].

Similarly, in pack desiccation results in frost formation on the product surface and internal package wall. This mechanism has been explained [6] as follows:

1. "If the outside temperature of a package decreases, then the inside surface of the package will drop below the product surface temperature leading to ice sublimation from product surface causing condensation onto the inside walls of the package".
2. "Similarly, when the outside temperature increases, the process is reversed and water vapor condenses on the product surface".
3. "As the freeze thaw cycling continues, the crystals on the product are more influenced by the package temperature than the product mass. This results in further sublimation of ice from product surface

to the package surface. Eventually this results in frost formation on the package”.

A folding carton used as a frozen food package can be adversely affected by water uptake from the food product inside. The paperboard fibers can swell. This causes deformity in the folding carton structure leading to carton damage. Both water migration and in-pack desiccation are affected by product surface area to volume ratio. A high ratio makes a frozen food package more susceptible to larger crystal formation and greater frost formation on both product surface and package wall. This can cause rapid deterioration in food quality and carton’s structural integrity.

Nearly 57% of supermarket returns are due to packaging damage caused during shipping, handling, receiving and stocking for the reasons mentioned above [2]. This makes it necessary to use a robust folding carton material to reduce unsaleables due to carton damage. A major material supplier produces a ‘Coated Natural Kraft’ (CNK) carton material topped with a proprietary coating known as ‘Custom Kote’. A research study done by an independent audit firm, showed that ‘Custom Kote’ carton board reduced frozen food unsaleables by 44% [2]. This study was done to determine if this damage reduction was at least partially due to enhanced compression strength compared to uncoated carton stock. This study compared the compression strength of folding cartons made from CNK (Coated Natural Kraft) SBS (Solid bleached sulfate), CRP (Coated recycled paperboard) and PCSBS (Poly coated solid bleach sulfate) after subjecting frozen pea filled cartons to multiple freeze-thaw cycles. The carton stock was procured from two different suppliers to eliminate material source bias in the findings of this study.

MATERIALS AND METHODS

Two sets of die cut carton blanks measuring 9 inch × 5 inch × 2-3/4 inch (22.8 cm × 12.7 cm × 6.9 cm) made from 4 different folding carton materials were provided by two suppliers. Proprietary coating was applied on the outside of carton. Carton board caliper, basis weight and stiffness were determined in accordance to standard test methods ASTM D 645/D 645M-97 [8], D 646 [9] and D5342-97 [10] respectively.

The folding cartons were sealed using a hot glue gun and a polyethylene base glue stick as the adhesive. Sealed cartons were pre-condi-

tioned according to ASTM D685 [11] prior to testing. Frozen peas were used as the product. They were purchased from a local grocery store and then packed into folding cartons. Frozen peas were packed in the cartons to provide a moisture source during the freeze/thaw cycle. Frozen peas were chosen to provide the maximum surface area to volume ratio, thus maximizing freeze-thaw cycling abuse of the folding cartons.

A top closing coffin freezer held at -18°C (Kelvinator, Cleveland, OH) was used for this study. A Lansmont "Squeezer" compression test system (Lansmont Corporation, CA) was used to determine the compression strength using a fixed platen moving at 0.5 in/min (1.27 cm/min). The software used to interpret peak load was a Squeezer Reader version 2.0.0. (Lansmont Corporation, Monterey, CA).

Cartons were filled with 900 grams of frozen peas with a 2 inch (5.04 cm) headspace (Figure 1). Cartons containing the frozen product were placed in the freezer on their 9 inch \times 2-3/4 inch (22.8 cm \times 6.9 cm) side to maximize freeze-thaw abuse on the four carton faces. Cartons were subjected to a freeze-thaw cycle of 23 hours at -18°C , and then 1 hour at 23°C and 50% RH for five days prior to compression testing. This condition was chosen on the basis of frozen distribution environment [12]. From a preliminary study it was determined that the cartons would be compression tested on the 9 inch \times 2-3/4 inch (22.8 cm \times 6.9 cm) face as it showed the least variation. In addition, the compression strength of empty folding cartons was measured to compare the differ-

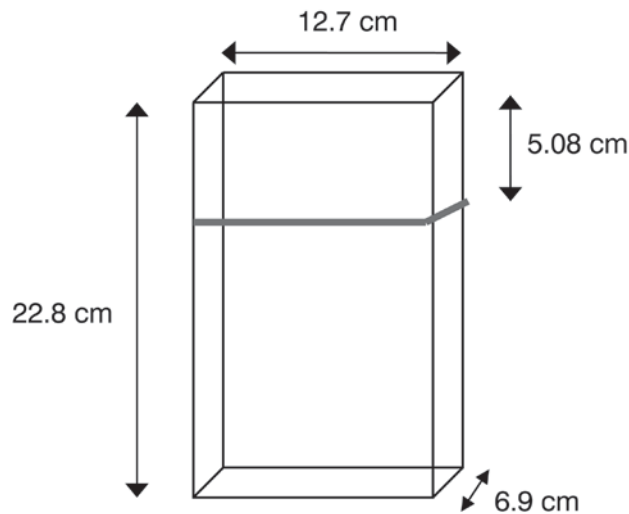


Figure 1. Fill height of frozen peas in the folding carton.

ent carton materials at ambient conditions (23°C, 50%RH) and to folding cartons subjected to freeze-thaw cycling.

Percent moisture content was determined for the four folding carton materials subjected to the three treatments. The three treatments were empty folding cartons; empty folding cartons subjected to five freeze-thaw cycles and pea filled folding cartons subjected five freeze-thaw cycles. For moisture analysis three carton samples weighing approximately 1.5 g were cut from three different locations from a folding carton. Two of the locations were from the carton faces 22.8 cm × 12.7 cm × 6.9 cm. The third location was on the opposite 22.8 cm × 12.7 cm face. Moisture content of the carton materials was determined according to ASTM D644 [13].

The data was analyzed using statistical software Minitab 13.1 by Minitab Inc, Pennsylvania. Analysis of variance was performed on the collected data for compression strength and percent moisture content. The means were separated using Fisher's LSD and the standard deviation for each treatment was noted.

RESULTS AND DISCUSSION

Carton material properties (basis weight and thickness) were determined prior to conducting the freeze-thaw experiments. It was found that the CNK provided by the first supplier had the highest basis weight (355.5 g/m²) followed by CRP, PCSBS and CSBS (Table 1). The CRP provided by the second supplier had the highest basis weight (382.2 g/m²) followed by CNK, PCSBS and CSBS. The thickness of all carton board material provided by both suppliers was measured to be approxi-

Table 1. Basis Weight and Thickness of Carton Material.

Carton Material	Supplier 1		Supplier 2	
	Basis Weight (g/m ²)	Thickness (mm)	Basis Weight (g/m ²)	Thickness (mm)
'Custom Kote' Coated Natural Kraft (CNK)	355.5	0.457	356.8	0.457
Coated Solid Bleached Sulfate (CSBS)	324.4	0.457	330.7	0.470
Coated Recycled Paperboard (CRP)	353.2	0.457	382.2	0.457
Polyethylene coated solid bleach sulfate (PCSBS)	350.6	0.457	357.2	0.495

mately 0.457 ± 0.00254 mm. Hence, the variation in carton material specifications was minimal between the two suppliers.

Under ambient test conditions (23°C, 50%RH) there was a significant difference ($p < 0.05$) in compression strength between the empty folding cartons made from the different carton materials from both suppliers (Figure 2 and 3). However cartons from both suppliers did not show a significant difference in compression strength between CNK and PCSBS empty cartons under ambient conditions. The highest average peak force was observed for cartons made from CNK at 283.3 N (Figure 2) for the first supplier and CRP at 274.3 N (Figure 3) for the second supplier. The lowest average peak force was significantly different from the highest average peak force for cartons made from CRP at 235.8 N (Figure 2) for the first supplier and CSBS at 245 N (Figure 3) for the second supplier. It was also observed that CNK folding carton had the highest bending stiffness in the cross direction compared to cartons made from CSBS, PCSBS and CRP (Table 2). The cartons were compressed top to bottom in the cross direction. Therefore, higher bending stiffness can contribute to a carton's compression strength [14]. So, it could be expected that prior to exposing folding cartons to a freeze-thaw test protocol, CNK cartons may have the highest compression strength at 21°C, 50% RH followed by SBS, PCSBS and CRP folding cartons.

As expected, after pea filled folding cartons were subjected to freeze/thaw cycling, the average peak force decreased for all carton materials compared to empty cartons tested at ambient conditions (Figures 2, 3, 4 and 5). This trend was observed in both suppliers. After testing there was a significant difference in the compression strength of cartons made from different carton materials (Figures 4 and 5). For both suppliers the highest average peak force was observed for cartons made from CNK (129.7 N and 139 N), which was significantly higher than the lowest average peak force for cartons made from PCSBS (45.9 N and 64.6N). Average peak force for CSBS and CRP were not significantly different from each other but were significantly lower than the average peak

Table 2. Bending Stiffness of Different Carton Materials.

Folding Carton	Machine Direction (TBU)	Cross Direction (TBU)
CNK	170.2	98.3
CSBS	152.9	83.4
CRP	176.8	55.1
PCSBS	165.0	83.1

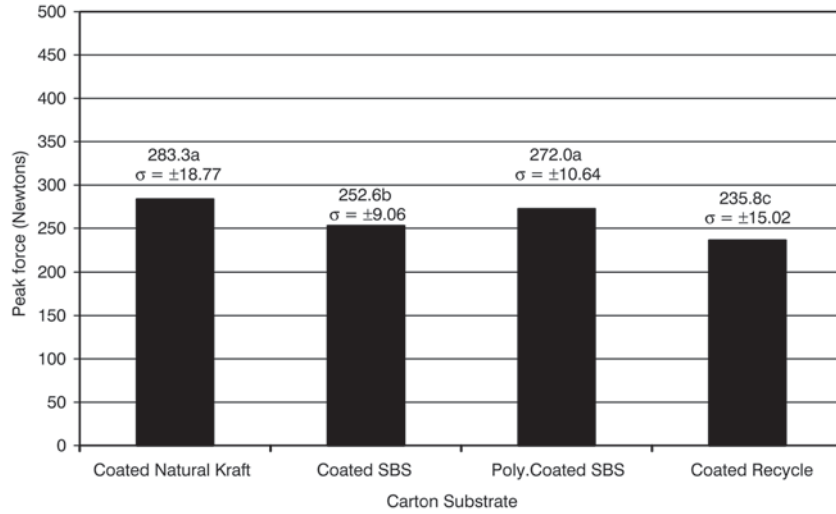


Figure 2. Compression strength of empty cartons at ambient conditions (Supplier 1). Means with different letters are significantly different ($p < 0.05$).

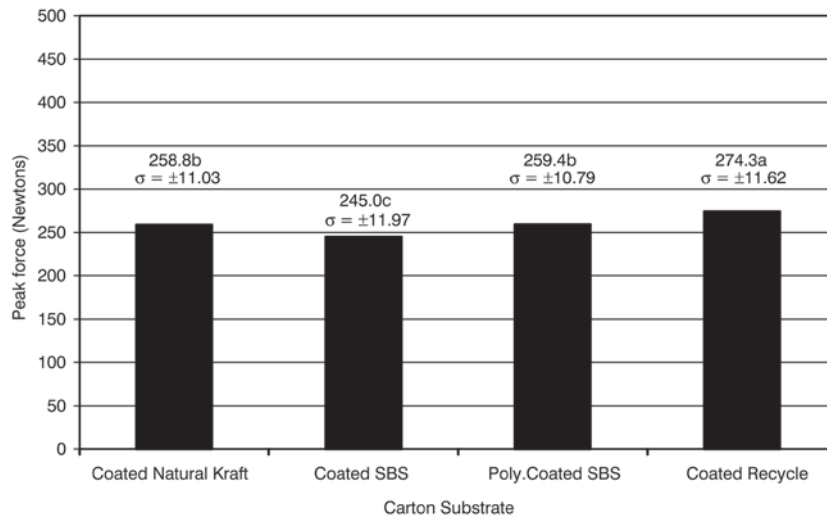


Figure 3. Compression strength of empty Cartons at ambient conditions (Supplier 2). Means with different letters are significantly different ($p < 0.05$).

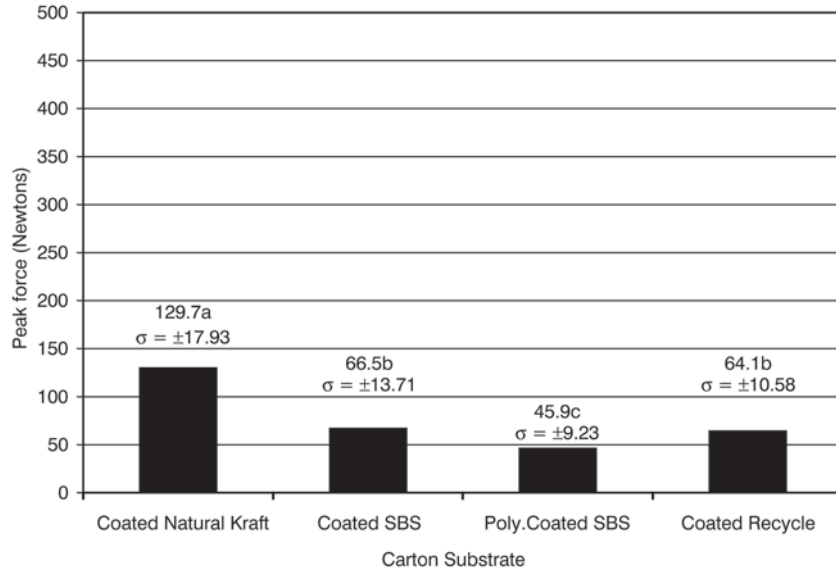


Figure 4. Compression strength of cartons after freeze-thaw cycling (Supplier 1). Means with different letters are significantly different ($p < 0.05$).

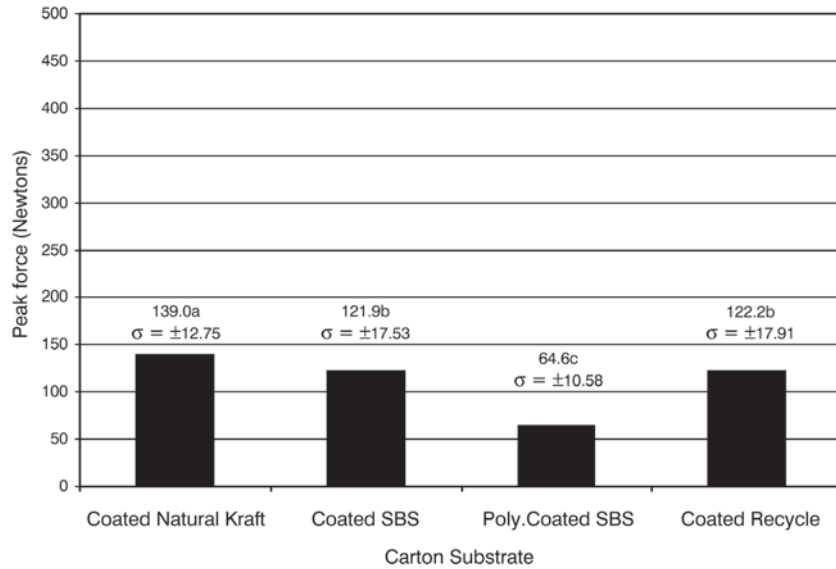


Figure 5. Compression strength of cartons after freeze-thaw cycling (Supplier 2). Means with different letters are significantly different ($p < 0.05$).

force of CNK cartons. CSBS and CRP folding cartons performed better than PCSBS cartons and had significantly higher average peak force than PCSBS cartons (Figures 4 and 5).

It should be noted that comparing the compression strength between cartons made from the same material but procured from different sources did not show a significant difference (Figures 4 and 5). Moreover, the type of carton material had an effect on the compression strength of carton after freeze-thaw abuse. The results show that after exposing pea filled cartons to a freeze-thaw test, CNK cartons had the highest compression strength followed by CSBS, CRP and PCSBS folding cartons (Figures 4 and 5).

Moisture analysis of the carton stock was performed to determine the effect of water migration and in-pack desiccation on the compression strength of cartons. The standard deviation across all treatments and carton materials was low. There was a considerable difference in moisture content between empty carton stock at 23°C, 50% RH and frozen pea filled folding carton stock subjected to freeze/thaw test (Figures 6 and 7). Frozen pea filled carton stock had higher moisture content than empty cartons. The multiple freeze-thaw empty (MFT Empty) carton stock did not have considerably higher moisture content than 'Empty' carton stock. Therefore, water migration into carton stock was due primarily to the product inside the carton and not from the carton's surroundings during the thawing phase of the FT cycle. This is evident from the percent moisture content of the empty carton stock exposed to FT cycles (Figures 6 and 7). This increase in moisture content most likely occurred due to water migration from frozen peas during the multiple freeze-thaw (MFT) cycling. Also, there was a significant difference in moisture content between cartons made from different carton materials. CNK carton stock had the lowest moisture content for treatment 'MFT Peas' (Figures 6 and 7). PCSBS carton stock (frozen pea filled carton) was observed to have the highest moisture content (Figures 6 and 7) after FT cycling. It should be noted that the moisture content of peas used for supplier 1 and supplier 2 were different, so there is a difference in the moisture uptake for the same material between the two suppliers (Figures 6 and 7). Keeping in view the above observations, this suggests that 'CNK' is a more robust material that can withstand temperature fluctuations during distribution.

There appears to be an inverse relationship between material moisture content and carton compression strength. With increasing moisture content there is a decrease in compression strength of cartons made

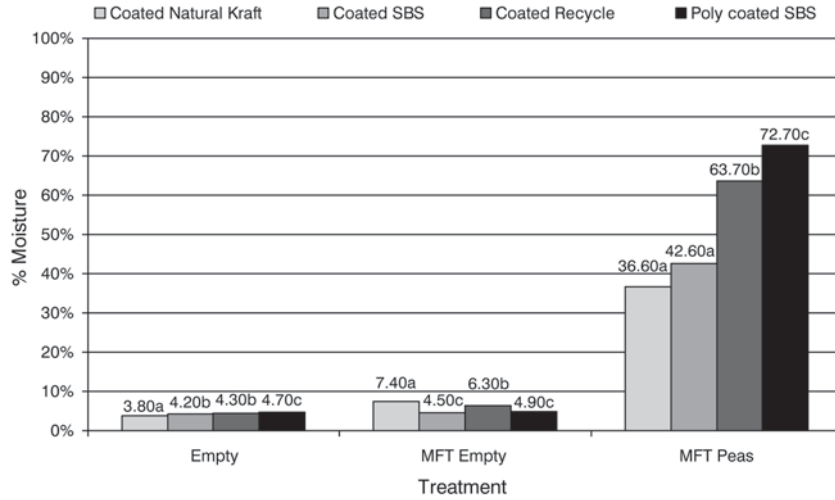


Figure 6. Moisture content (dry basis) of folding carton materials (Supplier 1). Means with different letters are significantly different ($p < 0.05$).

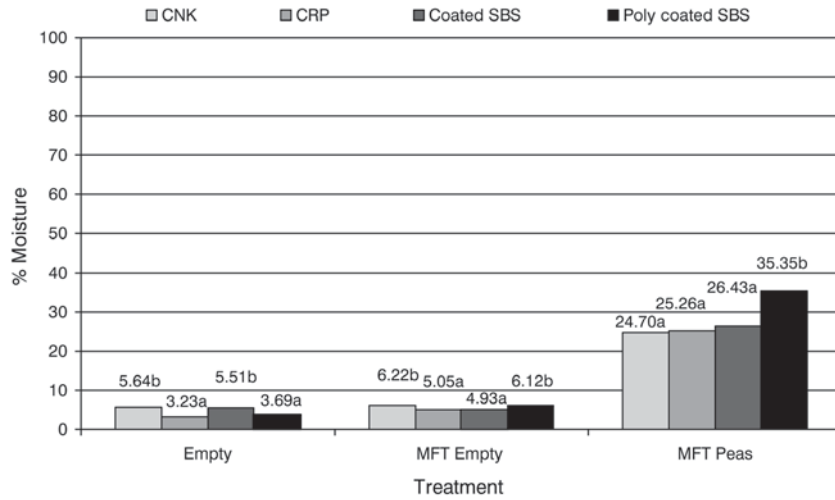


Figure 7. Moisture content (dry basis) of folding carton materials (Supplier 2). Means with different letters are significantly different ($p < 0.05$).

from different carton materials. It has been observed that moisture uptake is mainly from the peas inside the carton. Therefore the surface coating on the outer face does not play a major role against moisture absorption. This trend was observed for all carton types from both suppliers (Figure 8). There is a distinct difference between the carton materials, where frozen pea filled CNK cartons had the highest percent retained compression strength and the lowest moisture content following freeze/thaw cycling (Figure 8). Since, CNK has unbleached pine fibers with higher levels of natural, residual internal sizing, it will absorb less moisture compared to the other carton materials. The carton material had obstructed moisture ingress of condensed water droplets on the carton surface during FT cycling. Frozen pea filled PCSBS cartons had the lowest average peak force with the highest moisture content after FT cycling (Figures 4 and 5). Since the moisture uptake was observed to be from the inside of the carton, this explained adhesion failure in the PCSBS folding cartons between the polyethylene layer (inside layer of carton) and the SBS paperboard substrate (outside layer of carton). This resulted in the carton's poor performance during compression strength testing. It appears that irrespective of the carton material supplier, folding cartons made from CNK hold their structural integrity better in a frozen distribution network.

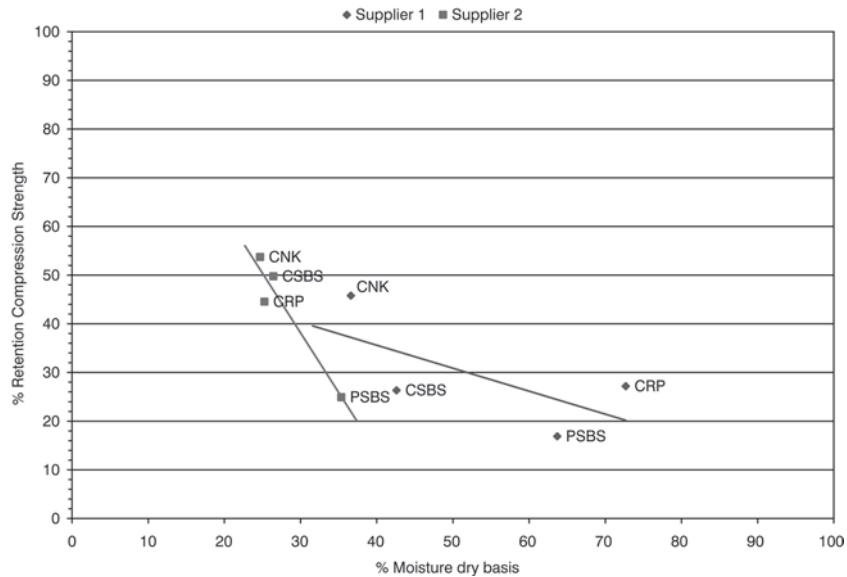


Figure 8. Effect of freeze-thaw cycling on compression strength of folding.

CONCLUSIONS

The higher bending stiffness of CNK (Table 2) can be attributed to longer fiber length compared to the other carton materials thus positively affecting carton compression strength. It was also observed that frozen pea filled CNK cartons subjected to freeze-thaw cycling had significantly higher capacity to withstand compression compared to folding cartons made from SBS, CRP and PCSBS (Figures 4 and 5). Multiple freeze-thaw cycling (Figure 8) of folding cartons resulted in increased moisture uptake and decreased compression strength. Since, frozen pea filled CNK cartons absorbed the least moisture from the inner surface of the carton during the multiple freeze-thaw cycling (Figure 8), they had the highest compression strength. Surface coating does not affect compression strength because moisture uptake is due to in pack desiccation as a result crystal formation on the inner surface of the carton. Coated Natural Kraft comprise of unbleached pine fibers providing stronger bonding sites compared to other carton materials thus retaining better dry value strength. This explains higher compression values for CNK cartons compared to SBS, CRP and PCSBS cartons, after multiple freeze-thaw cycling. It can be concluded that Coated Natural Kraft will provide more carton compression strength for packaging frozen food compared to folding cartons made from SBS, PCSBS and CRP.

REFERENCES

1. MeadWestvaco Research Proves CNK[®] Reduces Frozen Food Unsaleables. <http://www.meadwestvaco.com/coatedboard.nsf/v/news?OpenDocument>, 2005.
2. Cartonboard Change Makes Dollars and Sense. In Food and Drug Packaging; <http://www.fdp.com/content.php?s=FP/2005/04&p=21>, 2005.
3. Zaritzky, N. E., Ann, M.C., Calvelo, A Meat Science 1982, 12, 105.
4. Reid, D. S. Fundamental Physiochemical Aspects of Freezing. *Food Technology* 1983, 37, 110–115.
5. Martino, M. N., Zaritzky, N.E. Ice Crystal Size Modifications during Frozen Beef Storage. *Journal of Food Science* 1988, 53, 1631–1637.
6. Martino, M. N., Zaritzky, N.E. Ice Recrystallization in a Model System and in Frozen Muscle Tissue. *Cryobiology* 1989, 26.
7. IIR Recommendations For The Processing and Handling of Frozen Foods, 3rd ed.; International Institute of Refrigeration: Paris, France, 1986.
8. ASTM Standard D 645/645M 1997 (2007) “Standard Test Method for Thickness of Paper and Paperboard”. ASTM International. ASTM International, West Conshohocken, PA, 2007, DOI: 10.1520/D0645_D0645M-97R07.
9. ASTM Standard D646 1996 (2007), “Standard Test Method for Grammage of Paper and Paperboard (Mass Per Unit Area)”, ASTM International, West Conshohocken, PA, 2006, DOI: 10.1520/D0646-96R07.
10. ASTM Standard D 5342-1997 (2007) “Standard Test Method for Resistance to Bending of

Paper and Paperboard” ASTM International, West Conshohocken, PA,2007, DOI: 10.1520/D5342-97R07.

11. ASTM Standard D 685 1993 (2007) “Standard Practice for Conditioning Paper and Paper Products for Testing”. ASTM International, West Conshohocken, PA, 2007, DOI:10.1520/D0685-93R07.
12. Wells J.H. and Singh R.P. ‘Performance evaluation of time-temperature indicators for frozen food transport’ *Journal of Food Science*, 2006; 50:2: pp 369–371.
13. ASTM Standard D 644 1999 (2007) “Moisture Content of Paper and Paperboard by Oven Drying”. ASTM International. ASTM International, West Conshohocken, PA,2007, DOI: 10.1520/D0644-99R07.
14. Beldie L.; Sandberg G.; Sandberg L. ‘Paperboard packages exposed to static loads–finite element modeling and experiments’ *Packaging Science and Technology* 2001; 14:4: pp 171–178.

Guide to Authors

1. Manuscripts shall be sent electronically to the editors, Changfeng Ge at cfgmet@rit.edu and Bruce Welt at bwelt@ufl.edu using Microsoft Word in an IBM/PC format. If electronic submission is not possible, three paper copies of double-spaced manuscripts may be sent to Changfeng Ge, Editor of the *Journal of Applied Packaging Research*, Rochester Institute of Technology, One Memorial Drive, Rochester, NY 14623-5603, USA (Telephone 585-475-5391) or Bruce Welt, Editor of the *Journal of Applied Packaging Research*, University of Florida, Box 110570, Gainesville, FL 32611-0570, USA (Telephone 352-392-1864, X-111). Manuscripts should normally be limited to the space equivalent of 6,000 words. The editor may waive this requirement in special occasions. As a guideline, each page of a double-spaced manuscript contains about 300 words. Include on the title page the names, affiliations, and addresses of all the authors, and identify one author as the corresponding author. Because communication between the editor and the authors will be electronic, the email address of the corresponding author is required. Papers under review, accepted for publication, or published elsewhere in journals are normally not accepted for publication in the *Journal of Applied Packaging Research*. Papers published as proceedings of conferences are welcomed.
2. Article titles should be brief, followed by the author's name(s), affiliation, address, country, and postal code (zip) of author(s). Indicate to whom correspondence and proofs should be sent, including telephone and fax numbers and e-mail address.
3. Include a 100-word abstract and keywords.
4. If electronic art files are not supplied, submit three copies of camera-ready drawings and glossy photographs. Drawings should be uniformly sized, if possible, planned for 50% reduction. Art that is sent electronically should be saved in either a .tif or .JPEG files for superior reproduction. All illustrations of any kind must be numbered and mentioned in the text. Captions for illustrations should all be typed on a separate sheet(s) and should be understandable without reference to the text.
5. DEStech uses a numbered reference system consisting of two elements: a numbered list of all references and (in the text itself) numbers in brackets that correspond to the list. At the end of your article, please supply a numbered list of all references (books, journals, web sites etc.). References on the list should be in the form given below. In the text write the number in brackets corresponding to the reference on the list. Place the number in brackets inside the final period of the sentence cited by the reference. Here is an example [2].

Journal: 1. Halpin, J. C., "article title", *J. Cellular Plastics*, Vol. 3, No. 2, 1997, pp. 432–435.

Book: 2. Kececioglu, D. B. and F.-B. Sun. 2002. *Burn-In Testing: Its Quantification and Optimization*, Lancaster, PA: DEStech Publications, Inc.

6. Tables. Number consecutively and insert closest to where first mentioned in text or type on a numbered, separate page. Please use Arabic numerals and supply a heading. Column headings should be explanatory and carry units. (See example at right.)
- | Resin System | Core Temp. (DSC peak) | Char Yield, % |
|-----------------|-----------------------|---------------|
| Epoxy (MY720) | 235 | 30 |
| C379: H795 = 14 | 285 | 53 |
7. Units & Abbreviations. SI units should be used. English units or other equivalents should appear in parentheses if necessary.
 8. Symbols. A list of symbols used and their meanings should be included.
 9. Page proofs. Authors will receive page proofs by E-mail. Proof pages will be in a .PDF file, which can be read by Acrobat Reader. Corrections on proof pages should be limited to the correction of errors. Authors should print out pages that require corrections and mark the corrections on the printed pages. Pages with corrections should be returned by FAX (717-509-6100) or mail to the publisher (DEStech Publications, Inc., 439 North Duke Street, Lancaster, PA 17602, USA). If authors cannot handle proofs in a .PDF file format, please notify the editors, Changfeng Ge at cfgmet@rit.edu or Bruce Welt at bwelt@ufl.edu.
 10. Index terms. With proof pages authors will receive a form for listing key words that will appear in the index. Please fill out this form with index terms and return it.
 11. Copyright Information. All original journal articles are copyrighted in the name of DEStech Publications, Inc. All original articles accepted for publication must be accompanied by a signed copyright transfer agreement available from the journal editor. Previously copyrighted material used in an article can be published with the *written* permission of the copyright holder (see #14 below).
 12. Headings. Your article should be structured with unnumbered headings. Normally two headings are used as follows:
Main Subhead: DESIGN OF A MICROWAVE INSTALLATION
Secondary Subhead: Principle of the Design Method
 13. If further subordination is required, please limit to no more than one (*Third Subhead*).
 14. Equations. Number equations with Arabic numbers enclosed in parentheses at the right-hand margin. Type superscripts and subscripts clearly above or below the baseline, or mark them with a caret. Be sure that all symbols, letters, and numbers are distinguishable (e.g., "oh" or zero, one or lowercase "el," "vee" or Greek nu).
 15. Permissions. The author of a paper is responsible for obtaining releases for the use of copyrighted figures, tables, or excerpts longer than 200 words used in his/her paper. Copyright releases are permissions to reprint previously copyrighted material. Releases must be obtained from the copyright holder, which is usually a publisher. Forms for copyright release will be sent by the editor to authors on request.

General: The *Journal of Applied Packaging Research* and DEStech Publications, Inc. are not responsible for the views expressed by individual contributors in articles published in the journal.